Preprint (invited review article), to appear in Handbook of Nanophysics 4 : Nanotubes and Nanowires, ed. K. D. Sattler, CRC press, (2010).

Ultrathin gold nanowires

Takeo Hoshi

Department of Applied Mathematics and Physics,

Tottori University, Tottori 680-8550, Japan

Yusuke Iguchi

Department of Applied Physics, The University of Tokyo,

Bunkyo-ku, Tokyo 113-8656, Japan

(Present address: Central Research Laboratories,

NEC Corporation, 1753, Shimonumabe,

Nakahara-Ku, Kawasaki, Kanagawa 211-8666, Japan)

Takeo Fujiwara

Center for Research and Development of Higher Education,

The University of Tokyo, Bunkyo-ku, Tokyo 113-8656, Japan

Abstract

A review is given for the physics of ultrathin gold nanowires; nanowire with a couple of atoms in their wire diameter and monoatomic chain. The beginning part gives a tutorial of solid state gold with related materials. The explanation is based on quantum mechanics of electrons and is crucial for understanding nanowire properties. Next, properties of gold and other metal nanowires are reviewed for fabrication, observation and theory. Appearance of monoatomic chain and quantized conductance at room temperature are focused on. The rest of the article is devoted to helical multishell nanowires, a unique property of gold. The observed multishell configurations are limited to specific ones with 'magic numbers'. Their formation mechanism is explained by a proposed theory and confirmed by quantum mechanical molecular dynamics simulation, atomistic simulation with quantum mechanical treatment of electrons. Finally, the helical multishell gold nanowire is discussed from a general scientific viewpoint and a future aspect is addressed so as to establish the foundation of nano electronics.

KEYWORD : gold, ultrathin nanowire, quantized conductance, helical structure, quantum mechanical molecular dynamics simulation

Contents

I. INTRODUCTION

Ultrathin nanowires of gold and other metals have been studied intensively, particularly from 1990's, as a possible foundation of nano electronics. See a review. [Agraït *et al.* 2003] They are fabricated as nano-meter-scale contacts within two electrode parts and are composed of a couple of atoms in their wire length and/or diameter. Monoatomic chain, the thinnest wire, was also fabricated. The metal nanowires can show quantized conductance, even at room temperature, which is completely different from Ohm's law in macroscale samples. Structural and transport properties of nanowires were investigated by (i) fine experiments, such as high-resolution transmission electron microscopy (HRTEM), scanning tunneling microscope (STM) and atomic force microscopy (AFM) and (ii) atomistic simulations with quantum-mechanical theory of electrons. Many experiments and simulations lead us to several common understandings among metal nanowires of various elements. [Agraït *et al.* 2003]

This article focuses on unique properties of gold nanowire. Common properties between gold and other nanowires are also discussed so as to figure out the uniqueness of gold nanowire in a general scientific viewpoint.

As a unique and fascinating property of gold nanowire, helical multishell structure was reported in 2000 [Kondo and Takayanagi 2000], as in carbon nanotube. [Iijima 1991, Dresselhaus *et al.* 2001] A shell of helical gold nanowires consists of a folded hexagonal sheet, while carbon nanotube [Iijima 1991, Dresselhaus *et al.* 2001] consist of a folded graphene sheet. This article focuses particularly on the helical multishell nanowire of gold both for phenomena and proposed formation mechanism. The discussion is based on electronic structure and covers a wide range of nano structures of gold and other metals.

This article is organized as follows; Section II is devoted to a tutorial for atomic structure and electronic wavefunctions of solid gold with other materials. Section III describes a summary of structure and transport properties of gold and other metal nanowires. Section IV focuses the helical multishell gold nanowire, as the main topic of the present article. Finally, in Sec. V, a summary of the article is given and a future aspect is addressed for establishing the foundation of nano electronics. Appendix is devoted to quantum-mechanical molecular dynamics (QM-MD) simulation, which is important for understanding points of this article.

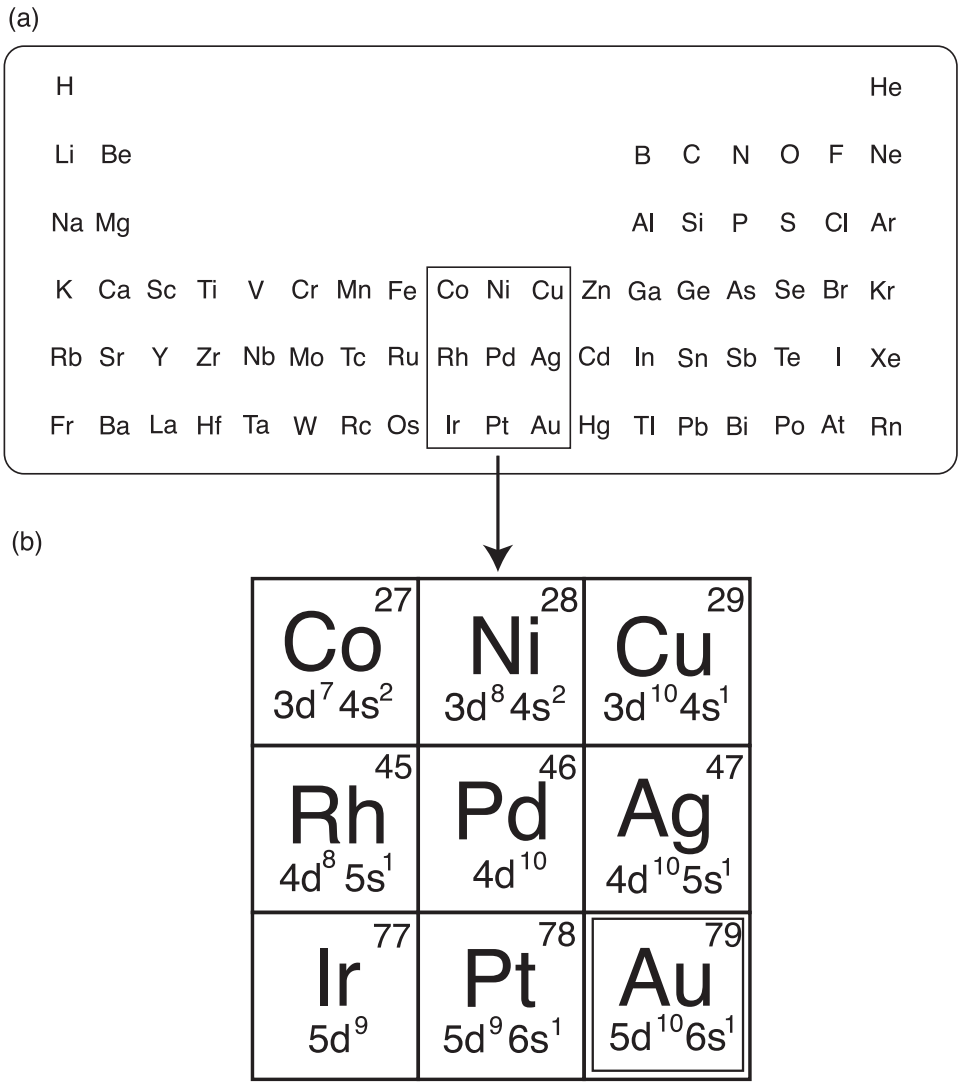

FIG. 1: (a) Periodic Table up to Period 6 elements. (b) A part of Periodic Table that contains gold (Au). The atomic number is plotted at the upper right corner of each box and the valence electron configuration is plotted at the lower area of each box. All the elements shown in (b) form FCC structure in solid state, except cobalt (Co).

II. BASIC PROPERTIES OF SOLID GOLD

Basic properties of gold (Au) are summarized with those of other elements. Figure 1 shows (a) Periodic Table up to Period 6 elements and (b) a part of Periodic Table that includes gold. Several elements in Fig. 1(b) will be discussed in this article. Among the elements, copper (Cu), silver (Ag) and gold are called noble metals. They have ten n d electrons and one $(n+1)$ s electron ($nd^{10}ns^1$) as valence electrons at each atom, where $n = 3, 4, 5$ for Cu, Ag and Au, respectively. The labels of 's' and 'd' indicate character of atomic orbitals. In general, an atomic orbital is described as

$$R(r)Q(\theta, \phi) \tag{1}$$

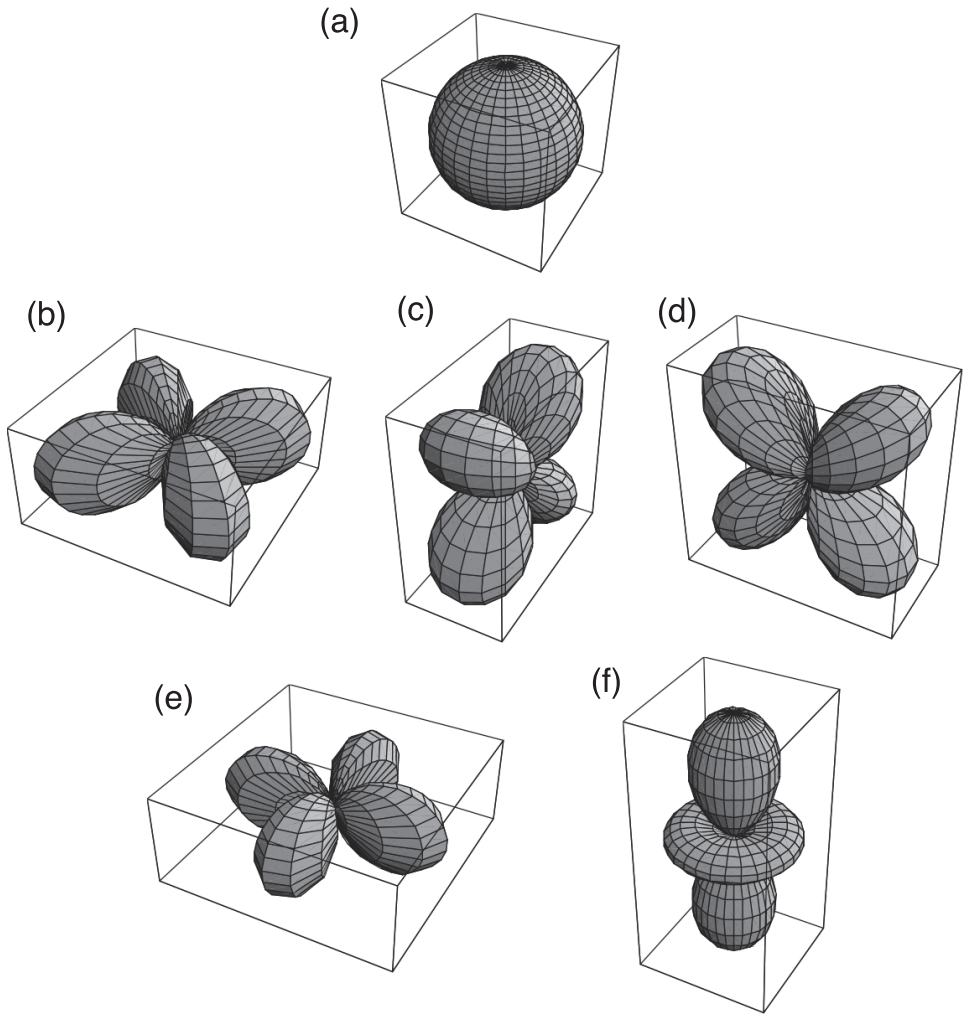

FIG. 2: Schematic figure of the non-spherical forms $|Q(\theta,\phi)|$ of (a) s orbital and (b)-(f) five d orbitals; (b)xy orbital, (c)yz orbital,(d)zx orbital,(e)x^2-y^2 orbital, (f)$3z^2-r^2$ orbital. The xy orbital spreads mainly on the xy plane.

in polar coordinate. The non-spherical distribution comes from the part of $Q(\theta,\phi)$. Wavefunction of s electron is spherical ($Q(\theta,\phi)$ =const) and that of d electron is not. Figure 2 illustrates the (non-)spherical distribution $Q(\theta,\phi)$ of s and d wavefunctions, by plotting the function of $r = r(\theta,\phi) \equiv |Q(\theta,\phi)|$. For example, the xy orbital spreads mainly on the xy plane. Another type of non-spherical atomic orbital, 'p' orbital, also appears later in this article. See elementary textbooks of quantum mechanics for details of the atomic orbitals.

All the elements in Fig. 1(b) form solid in face-centered-cubic (FCC) structure, shown in Fig. 3(a), except cobalt (Co) that forms close-packed hexagonal (HCP) structure. The lattice constant, the distance between the A and B atom in Fig. 3(a), is 3.61, 4.09 and 4.08 Å for copper, silver and gold, respectively. In this article, as in many textbooks, x, y, z axes are defined and normalized so that the cubic box

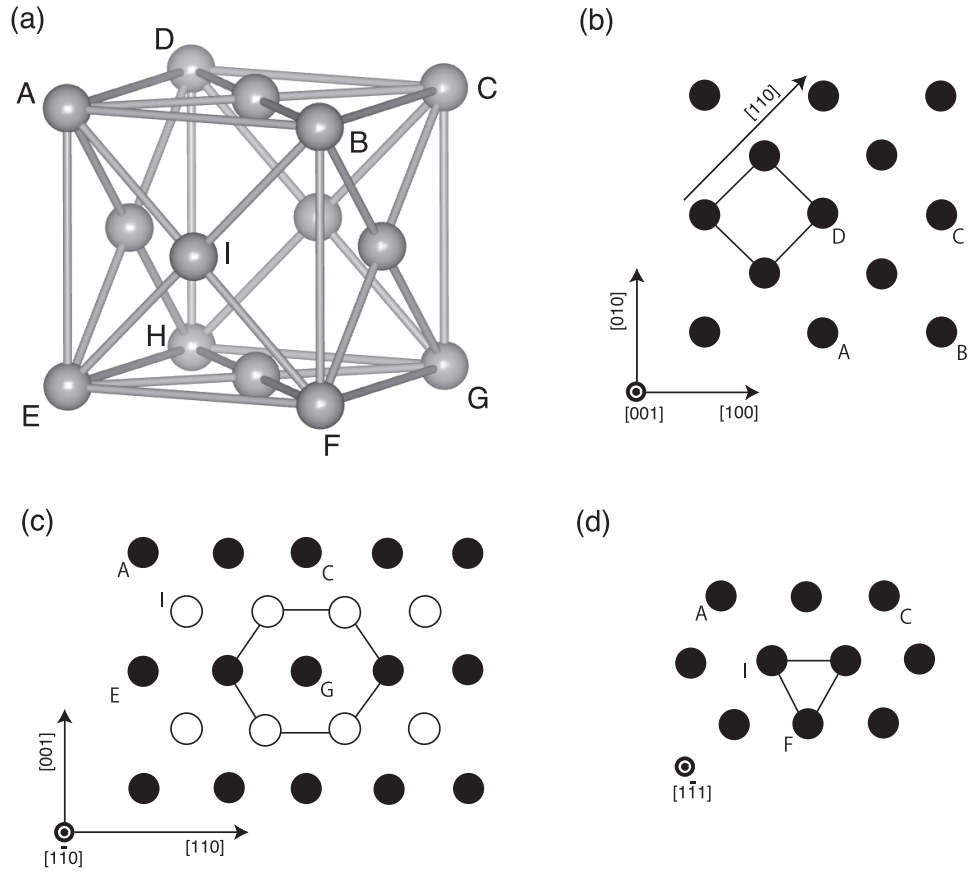

FIG. 3: (a) FCC structure. 'Bonds' are drawn between nearest neighbor atoms. (b) (001)-type, (c) (110)-type and (d) (111)-type planes of FCC structure. The atoms marked as A,B,C,D,E,F,G,H and I are common among the figures (a)-(d). Shapes drawn by lines in (b), (c) and (d) will appear later in this article. In (c), two successive atomic layers are drawn and the atoms in the two atomic layers are depicted by open and filled circles, respectively.

shown in Fig. 3(a) gives the cubic region of $0 \leq x, y, z \leq 1$. In Fig. 3(a), the eight corner atoms labeled by A, B, C, D, E, F, G and H are described, for examples, by $(1, 0, 0)$ and $(0, 1, 0)$ and the six face-center atoms, such as the atom I, are described, for examples, $(1/2, 1/2, 0), (0, 1/2, 1/2)$ in the normalized coordinate. FCC and HCP structures are ones in close packing (highest average density) as three dimensional lattice and each atom has twelve nearest neighbor atoms; For example, the atom placed at $(0, 0, 0)$ has the twelve nearest neighbor atoms that placed at $(\pm 1/2, \pm 1/2, 0), (\pm 1/2, 0, \pm 1/2), (0, \pm 1/2, \pm 1/2)$.

Several planes in the FCC structure are drawn in Figs. 3(b)-(d). Here the notations of planes are explained. A plane of $(x/l) + (y/m) + (z/n) = 1$ is indicated by an index of (l, m, n). The negative surface index is written with a bar; For example, the index of $(\bar{1}11)$ means the plane of $(x/(-1)) + (y/1) + (z/1) = 1$ or $-x + y + z = 1$. A direction vector is denoted as $[abc]$ and a '$[abc]$ nanowire' is a wire of which axis is in the $[abc]$ direction. Moreover, equivalent planes are called by 'type' in this article. For example,

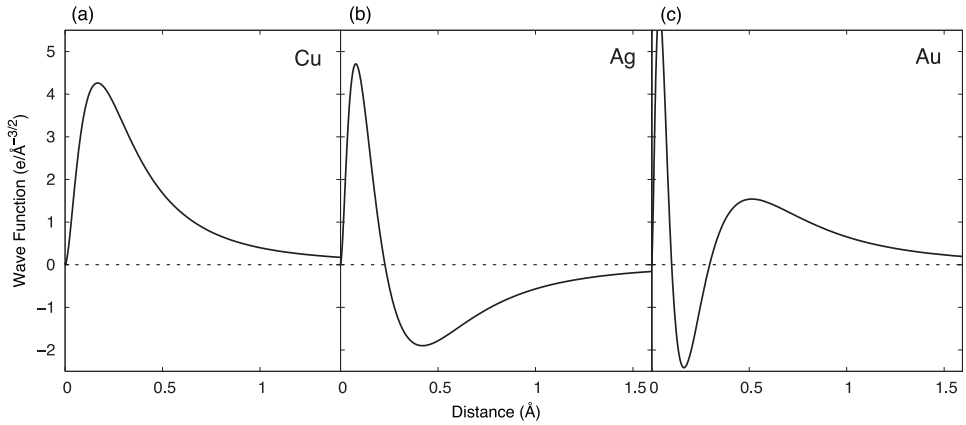

FIG. 4: Radial wavefunctions $R(r)$ of noble metals in the bulk FCC structure. See text for details.

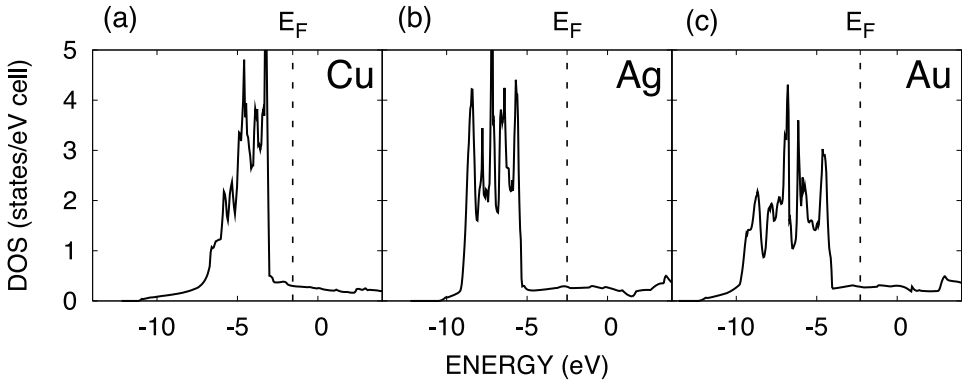

FIG. 5: Density of states, or energy spectrum of electronic states, in bulk FCC solids among noble metals. See text for details.

the lattice structures on (111) and ($\bar{1}$11) planes of FCC structure are equivalent to those shown in Fig. 3(d) and these planes are called '(111)-type' planes. The (001)-type, (110)-type and (111)-type planes are drawn in Fig.3(b), (c) and (d), respectively. A (111)-type plane has hexagonal structure with triangular tiles shown in Fig. 3(d) and is one in close packing as two-dimensional lattice.

Electronic states among noble metals in FCC solid are described in Figs. 4 and 5. The data are given by a modern quantum-mechanical calculation for electronic structure; The calculations are carried out by first-principles theory, the density functional theory with the linear-muffin-tin-orbital method [Andersen and Jepsen 1984]. See a text book[Martin 2004] for an overview of modern electronic structure theories. Since gold is a heavy element, relativistic effect is included in these calculations, as scaler-relativistic formulation. See textbooks of quantum mechanics, such as Ref. [Schiff 1968], for relativistic effect and scaler-relativistic formulation. Figure 4 shows the radial wavefunctions $R(r)$ of the d orbitals. An (nd) orbital has $(n-2)$ nodes in the radial wavefunction $R(r)$.

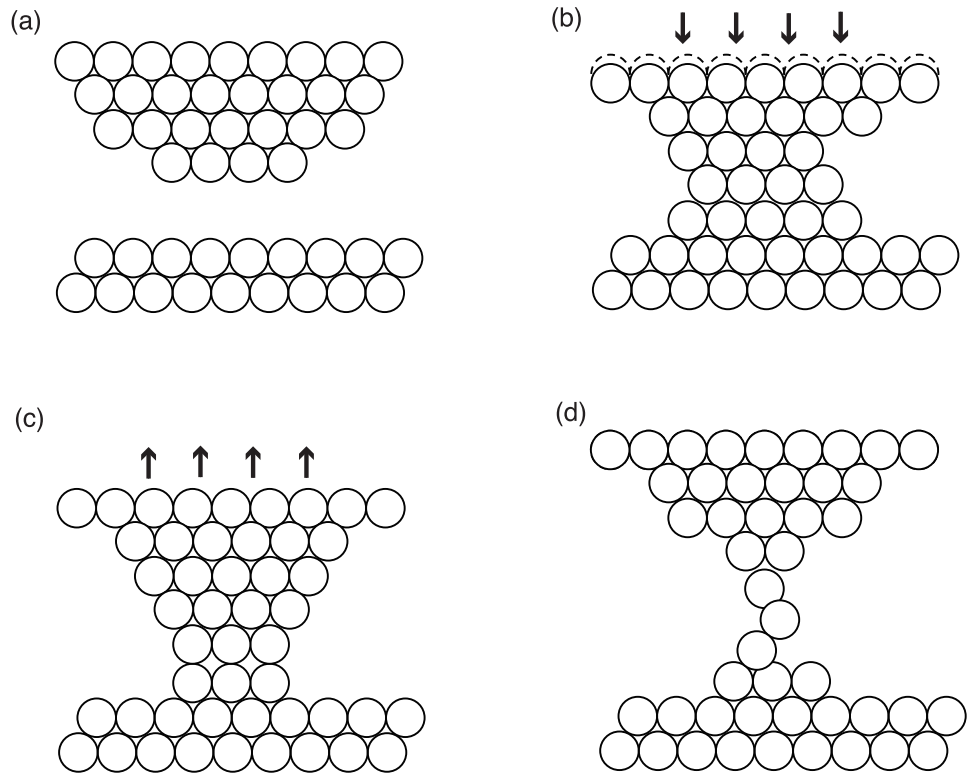

FIG. 6: Schematic figure of fabrication of nanowire using a STM tip. Atoms are depicted as balls.

The Cu wavefunction, an $3d$ wavefunction, does not have a node and the Ag and Au wavefunctions, $4d$ and $5d$ wavefunctions, have one and two node(s), respectively. Figure 5 shows the electronic density of states (DOS), or the energy spectrum of electronic states. The dashed line in Fig. 5 indicates the Fermi level $\varepsilon_{\rm F}$, which means that the electrons occupy the energy region of $E < E_{\rm F}$. As a common feature of the three elements, the d band is narrow and fully occupied, while the s band is broad and partially occupied. In the case of gold, for example, the d band lies in the narrow energy region of $-10{\rm eV} \leq E \leq -4{\rm eV}$, which is within the occupied energy region. The s band, on the other hand, lies in the region from -13eV up to the right end of the graph. The above feature indicates that the ten d electrons form a closed electronic shell and are nearly localized at atomic regions, while the one s electron is extended and can contribute to electrical current. Therefore, these solids are metallic and electrical current is observed with Ohm's law.

III. METAL NANOWIRE AND QUANTIZED CONDUCTANCE

Nanowires or nano-scale contacts of metals are fabricated by deformation processes with, for example, STM tip or mechanically controllable break junction.

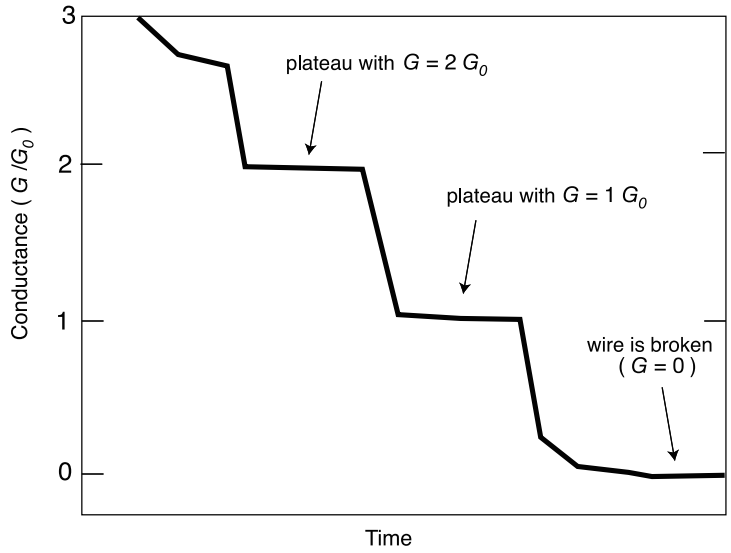

FIG. 7: Schematic figure of conductance trace in thinning process.

[Agraït *et al.* 2003] Fig. 6 illustrates the fabrication process by a STM tip, in which a nanowire is formed between two electrode parts. Real space image, like one in Fig. 6, is obtained by HRTEM. A formation process of a gold nanocontact was observed as successive HRTEM images [Kizuka *et al.* 1997, Kizuka 1998].

Quantized conductance of metal nanowire was reported, even at room temperature, and relatively clear quantized values were observed among noble metals and alkali metals. [Agraït *et al.* 2003, Agraït *et al.* 1993, Pascual 1993, Krans *et al.* 1993, Olesen *et al.* 1994, Krans *et al.* 1995, Brandbyge *et al.* 1985, Rubio *et al.* 1996, Muller *et al.* 1996, Costa-Krämer *et al.* 1997, Hansen *et al.* 1997, Yanson *et al.* 1999, Yanson *et al.* 2000, Yanson *et al.* 2001, Smit *et al.* 2003, Mares *et al.* 2004, Mares *et al.* 2005, Bettini *et al.* 2005] The quantized conductance G is defined as

$$G = nG_0, \tag{2}$$

where n is an integer and

$$G_0 \equiv \frac{2e^2}{h} \tag{3}$$

is the conductance unit defined by the charge of electron $e(>0)$ and Planck's constant h. Figure 7 is a schematic figure of conductance trace in thinning process, such as the process of Figs. 6(c) and (d). In Fig. 7, conductance plateaus of $G \approx 2G_0, 1G_0$ appear and the conductance reaches $G \approx 0$, when the wire is broken. In experimental research,

histogram of conductance values is constructed from many independent samples and a sharp peak at an integer value ($G = nG_0$) in the histogram is assigned to be a quantized conductance.

Simultaneous observation of structure and transport was realized by combined experiment of HRTEM and STM (TEM-STM) [Ohnishi and Takayanagi 1998, Erts *et al.* 2000, Kizuka *et al.* 2001a], which is crucial for understanding nanowires, because the conductance value, in general, does not determine atomic structure uniquely. A TEM-STM experiment in 1998 [Ohnishi and Takayanagi 1998] obtained a direct image of a monoatomic gold chain with the length of several atoms and observed a quantized conductance in $G = G_0$.

Force measurement was realized by combined experiment of AFM and STM [Rubio *et al.* 1996] and shows that a jump in conductance trace occurs with a jump in the force. The result implies that a jump in conductance trace is caused by plastic deformation of nanowire. Stress-strain curve was obtained by combined experiment of TEM and AFM [Kizuka *et al.* 2001b, Erts *et al.* 2002, Kizuka 2008] and the above statement was confirmed. In addition, simultaneous measurement of stiffness and conductance was realized by mechanically controllable break junction with a force sensor and applied to gold and platinum nanowires. [Rubio-Bollinger *et al.* 2004, Valkering *et al.* 2005, Shiota *et al.* 2008]

Quantum mechanical theory of electrical current has a rigorous foundation of non-equilibrium Green's function, which can be seen in a textbook. [Datta 1995] Here only a resultant formulation is briefly explained. In quantum mechanics, electrons are described as 'waves' with discretized energy levels and electrical current is given by the 'wave modes' that are extended through nanowire. Such extended 'wave modes' are usually called channels. The integer n in Eq. (2) is the number of the channels. A general expression of the conductance is

$$G = G_0 \sum_i \tau_i, \tag{4}$$

where τ_i is the transmission rate of the i-th 'wave mode' ($0 \leq \tau_i \leq 1$). [Datta 1995] Equation (4) will be reduced to Eq. (2), when all the channels are perfectly ballistic ($\tau_i = 1$).

Simulation of atomic structure is crucial for metal nanowire, since the transport properties are sensitive to atomic structure. A pioneering theoretical work in 1993 [Todorov *et al.* 1993] investigated the relation between atomic structure and the

conductance, in which the dynamics of atomic structure is determined by a classical potential. Nowadays, quantum mechanical molecular dynamics (QM-MD) simulation is a standard simulation tool for nanowire and other nanostructures. In QM-MD simulations, an effective Schrödinger equation is solved at each time step and atomic structures are updated under the change of electronic states. See Appendix A for a tutorial of QM-MD simulation. QM-MD simulation enables us to investigate (i) simultaneous discussion of structure and electronic properties in a single theoretical framework with quantum mechanics of electrons and (ii) systematic research among various elements. Many simulations were carried out for monoatomic gold chain and related materials. [Agraït *et al.* 2003, Brandbyge *et al.* 1985, Brandbyge *et al.* 1999, Okamoto and Takayanagi 1999, da Silva *et al.* 2001, Fujimoto and Hirose 2003, da Silva *et al.* 2004] After intensive works of simulation and experiment, it is established that a monoatomic gold chain is formed and shows a quantized conductance of $G = 1G_0$, since only one s orbital contributes to the current.

'Thicker' nanowires, nanowires thicker than monoatomic chain, can show complex structural and/or transport properties. An interesting viewpoint is shell effect that enhances the stability of specific integer values in the conductance. The conductance histograms in alkali and noble metals were analyzed from the viewpoint of the shell effect. [Yanson *et al.* 1999, Yanson *et al.* 2000, Yanson *et al.* 2001, Mares *et al.* 2004, Mares *et al.* 2005] In the context of the shell effect of alkali and noble metals, the stability of elliptical metal nanowires was investigated quantum mechanically within a free-electron model in continuum media. [Urban *et al.* 2004] Other theoretical investigations with free-electron models are found in the reference lists of the above papers or a review. [Agraït *et al.* 2003] It is noteworthy that a difference of alkali and noble metals is the fact that the valence band of alkali metals consists of one s electron, while that of noble metals consists of one s electron and ten d electrons, as shown in Fig. 5. A TEM-STM experiment was carried out with thicker [110] gold nanowires for the direct relation between the structure (the shape of the cross section) and the conductance. [Kurui *et al.* 2007] The appearance of helical multishell gold nanowire [Kondo and Takayanagi 2000] is a fascinating property of 'thicker' nanowires and will be discussed in the rest of the present article. As another systematic research of 'thicker' nanowires, a TEM-STM experiment was carried out for gold nanocontacts parallel to the [001], [111] and [110] directions.[Oshima *et al.* 2003a] The paper suggests that the variety in the crystalline orientation of the contacts can be the origin of the observed variety in the conductance trace among samples. The sliding of a twin boundary in

a gold nanocontact was reported by direct HRTEM observation. [Kizuka 2007] A recent TEM-STM experiment [Kurui *et al.* 2008] found (111)-type and (001)-type atomic sheets between electrode parts and they show quantized conductance.

To end up this section, brief comments are made on metal nanowires in which p and d orbitals contribute to current. Such nanowires can show a complex transport behavior, even in monoatomic chains. For example, nanowires of aluminum has s and p valence orbitals and show that plateau structure in conductance trace is less regular but the plateaus-like structures are still observed nearly at integer conductance values. [Krans *et al.* 1993, Cuevas *et al.* 1998, Yanson *et al.* 2008] In nanowire of nickel, a transition metal, the quantized conductance changes systematically under varying external parameters, the temperature (above and below the Curie temperature) and the applied magnetic field. [Oshima and Miyano 1998]

IV. HELICAL MULTISHELL STRUCTURE

A. Overview

At the year of 2000, helical multishell gold nanowires were synthesized and observed by HRTEM image. [Kondo and Takayanagi 2000] They were fabricated by focusing electron beam on thin film. [Kondo and Takayanagi 1997] The wire axis of the helical nanowires is the [110]-type direction of the original FCC geometry (See Figs. 3(b) and (c)). The outermost shell is a folded (111)-type (hexagonal) atomic sheet (See Figs. 3(d)) and helical around the nanowire axis. A single shell helical structure was synthesized later. [Oshima *et al.* 2003b] Experiments also observed the thinning process [Oshima *et al.* 2003c] and the conductance [Oshima *et al.* 2006] of the multishell helical structures.

Hereafter a multishell structures is denoted by the numbers of atoms in each shell. For example, a '14-7-1 nanowire' is a rod with three shells in which the outer, middle and inner shells have fourteen, seven and one atom(s) in the section view, respectively. The shape of the '6-1 nanowire' is depicted by lines in Fig. 3(c).

The observed multishell configurations are quite specific and are characterized by 'magic numbers'. The multishell structures in the 7-1, 11-4, 13-6, 14-7-1, 15-8-1 structures were experimentally observed. These number are called 'magic numbers', since the difference of numbers between the outermost and the next outermost shells is seven, except the cases of the 7-1 structure. Such a rule of the observed multishell configurations

implies that there is an intrinsic mechanism to form the specific multishell configurations.

Transport property of helical multishell gold nanowire was investigated both in theory [Ono and Hirose 2005] and experiment [Oshima *et al.* 2006], which will be discussed in Sec. V.

The appearance of helical metal wires was investigated by simulations with different methodologies. Before the experimental report of helical gold nanowire (in 1998), various 'exotic' structures of nanowires were predicted with potentials of Al and Pb and one of them is helical structure. [Gülseren *et al.* 1998] After the experimental report, several investigations, such as Refs. [Bilalbegović 2003, Lin *et al.* 2005] were carried out with classical potentials. Quantum mechanical simulations were also carried out. [Tosatti *et al.* 2001, Senger *et al.* 2004, Yang *et al.* 2004] A first principles calculation reported that the tension of nanowires gives the minimum values when the number of atoms of the lateral atomic row on the outermost shell is seven and the nanowire is helical. [Tosatti *et al.* 2001] It is also showed that the tension does not have the minimum in model silver nanowires. Another first principles calculation was carried out for nanowires with atoms from three to five on the lateral atomic row on the outermost shell, and showed that helical nanowires are not the configuration of the minimum energy but of the minimum tension. [Senger *et al.* 2004] Although these studies gave important progress on theory, they did not explain why the helical structures are formed in the specific multishell configurations with 'magic numbers'.

Platinum (Pt) nanowires were also synthesized with the same type of helicity. [Oshima *et al.* 2002] Platinum is placed at a neighbor of gold in Periodic Table (See Fig. 1(b)) and its electronic configuration ($5d^9 6s^1$) is similar to that of gold ($5d^{10} 6s^1$). The above experiment implies that the mechanism of formation of helical nanowires is generic between gold and platinum and may be inherent among some other elements.

In 2007, a theory[Iguchi *et al.* 2007] was proposed for formation model of helical multishell nanowires. In the model, the transformation consists of two stages; At the first stage, the outermost shell is dissociated from the inner shell to move freely. At the second stage, an atom row slips on the wire surface and a (001)-type (square) face (Fig. 3(b)) transforms into a folded (111)-type (hexagonal) one (Fig. 3(d)) with helicity. The driving force for the helicity comes from the nature of non-spherical $5d$ electrons and a (111)-type surface structure is energetically favorable for $5d$ electrons. The theory contains the following points: (i) The theory explains the observed multishell configurations with 'magic numbers' systematically. (ii) The theory was confirmed by QM-MD simulations for gold and copper with tight-binding form Hamiltonian. (See Appendix

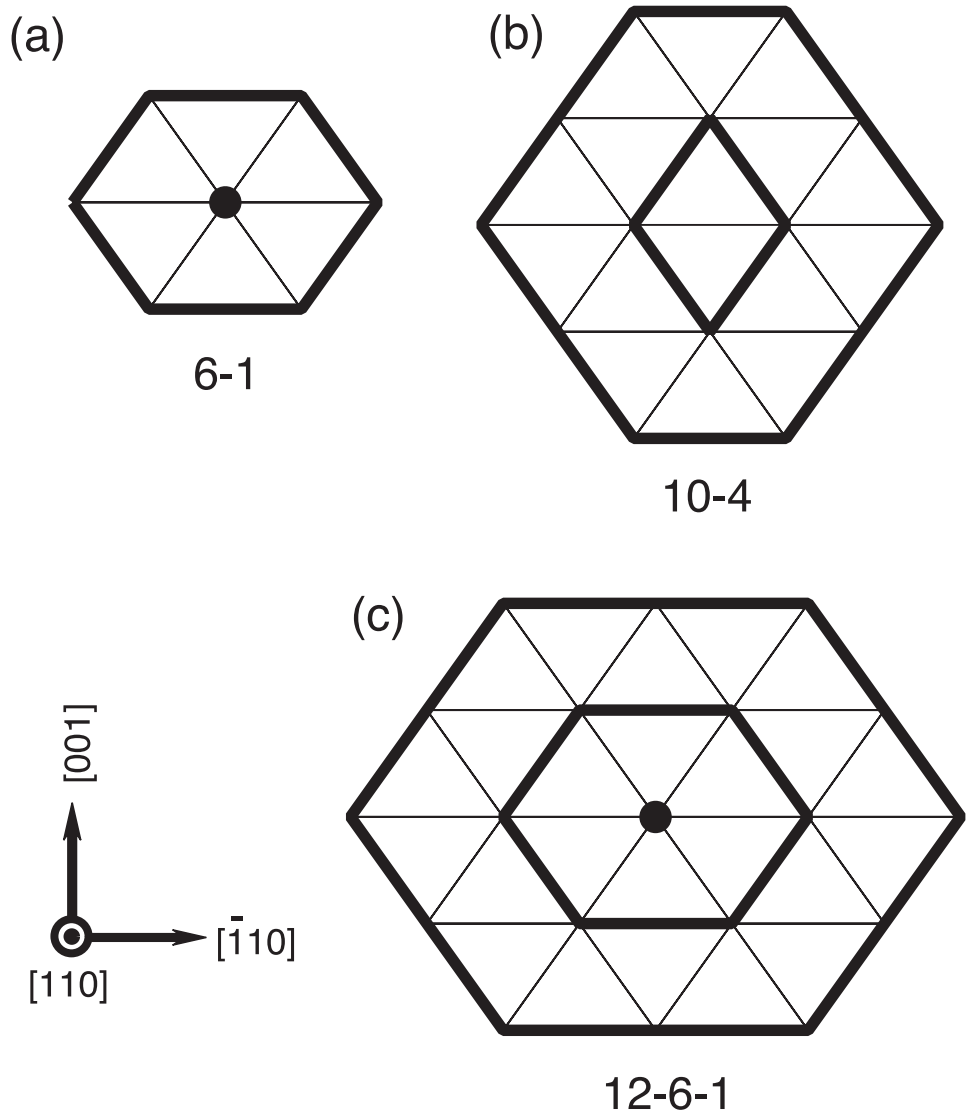

FIG. 8: Section view of a set of 'reference' [110] nanowires. The (a) 6-1, (b) 10-4 and (c) 12-6-1 structures are shown. See text for details. The shape of the 6-1 structure can be found in Fig.3(c).

A) (iii) The theory gives a general understanding among helical nanowire structures of gold and platinum and several reconstructed structures of equilibrium surfaces. After the proposal of the two-stage model [Iguchi *et al.* 2007], several related simulations were carried out for formation of helical gold nanowire within tight-binding form Hamiltonian. [Fujiwara *et al.* 2008, Amorim *et al.* 2008]

B. Two stage formation model

Hereafter, the multishell helical structures are systematically constructed, according to the proposed theory of two stage formation model. [Iguchi *et al.* 2007, Iguchi 2007]

First, a set of ideal [110] nanowires are prepared under the two conditions: (a) there

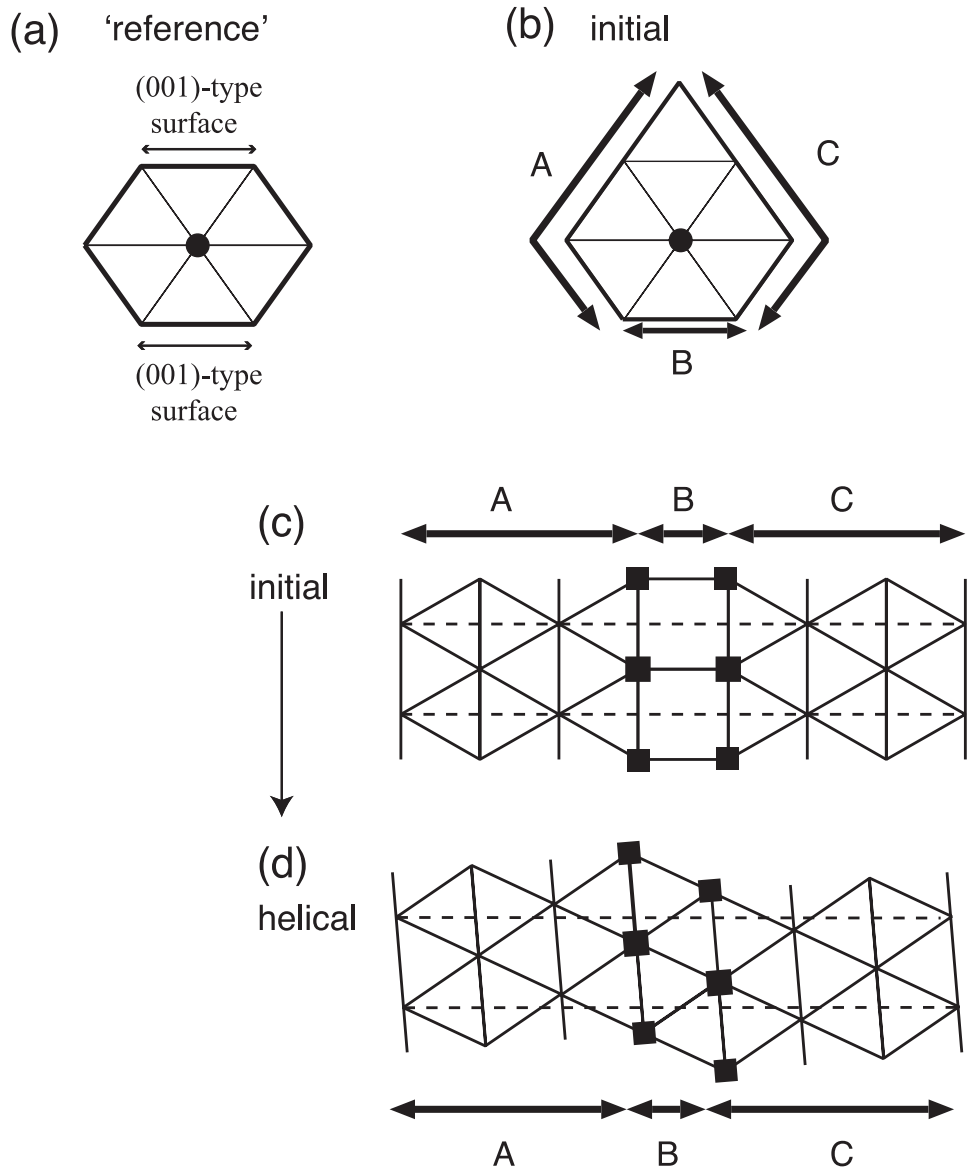

FIG. 9: Schematic figure of the formation of the helical 7-1 structure: (a) 'Reference' 6-1 structure. Two (001)-type surfaces appear and the other surfaces are (111)-type ones. (b) Initial 7-1 structure. The areas A and C are the (111)-type surfaces and the area B is the (001)-type surface. (c) Expanded lateral surface of the initial 7-1 structure of which the section view is given in (b). Dashed lines connect the same atoms at the right and the left ends. (d) Expanded lateral surface of the helical 7-1 structure transformed from the ideal non-helical structure of (c).

is no acute angle on the surface because of diminishing surface tension, and (b) there is no (001) side longer than any (111) side since the surface energy of a (001) surface is higher than that of (111). These structures are called 'reference' structure in the present article. Figure 8 shows the section views of the 'reference' structures in the 6-1, 10-4, and 12-6 multishell configurations. Among them, the outermost shell has six more 'bonds' on the lateral row than the inner shell, shown by bold lines in Fig. 8.

The formation process of the helical 7-1 structure is depicted schematically in Fig. 9.

When an atom row appears at a (001)-type surface on the outermost shell of the reference 6-1 structure (Fig. 9(a)), the structure turns into a 7-1 structure (Fig. 9(b)) and is called 'initial' structure in this article. The outermost shell has seven more atoms on a lateral atom row than the inner shell and the outermost shell can have room for atom row slip. This is the origin of the 'magic numbers'. Figure 9(c) shows an expanded lateral surface of the initial 7-1 structure. In Fig. 9(c), the surface region of B is (001)-type (square) lattice, while the surface regions of A and C are (111)-type (hexagonal) ones. Dashed lines connect the same atoms at the right and the left ends. When the number of atoms on the lateral row in the outermost shell is odd, the surface reconstruction brings the helicity to the nanowire inevitably; A slip of atom row transforms the surface region B from (100)-type surface into a folded (111)-type one with helicity. As result, the helical 7-1 structure is formed, as in Fig. 9(d).

C. Simulation of formation process

A QM-MD simulation was carried out, so as to confirm the proposed process model for forming helical structure. The simulation was carried out with a tight-binding form Hamiltonian that was used for several simulations of gold nanowire. [da Silva *et al.* 2001, da Silva *et al.* 2004] Details and theoretical foundations of the QM-MD simulations are described in Appendix. A Relaxation process with thermal fluctuation was simulated.

The samples in the simulations were finite [110] nanowires with the initial structures of the ideal 7-1, 10-4, 11-4, 12-6-1, 13-6-1, 15-7-1 and 15-8-1 structures. The simulation results are summarized in Fig. 10 as section views, except those of the 10-4 and 12-6-1 structures. The initial structures appear in the left panels of Figs. 10(a)-(e). They are 'reference' structures with one additional atom row on the outermost shell, as explained in the previous section. The additional atom rows are marked by arrows. The rod length is nine layers in the 7-1, 10-4 and 11-4 nanowires, seven layers in the 12-6-1 and 13-6-1 nanowires, or six layers in the 14-7-1, and 15-8-1 nanowires, respectively. Here the layer unit is defined as the periodic unit of the ideal FCC structure and is composed of two successive atomic layers shown in Fig. 3(c). The numbers of atoms in the simulations are from 76 to 156. The boundary condition is imposed by fixing the center of gravity of the top and bottom layers of the nanowires.

The finite-temperature dynamics is realized by the thermostat technique and the simulations were carried out at T =600 K and 900K, which are lower than the melting temperature (1337K). One iteration step corresponds to δt = 1 fs. Helical structures

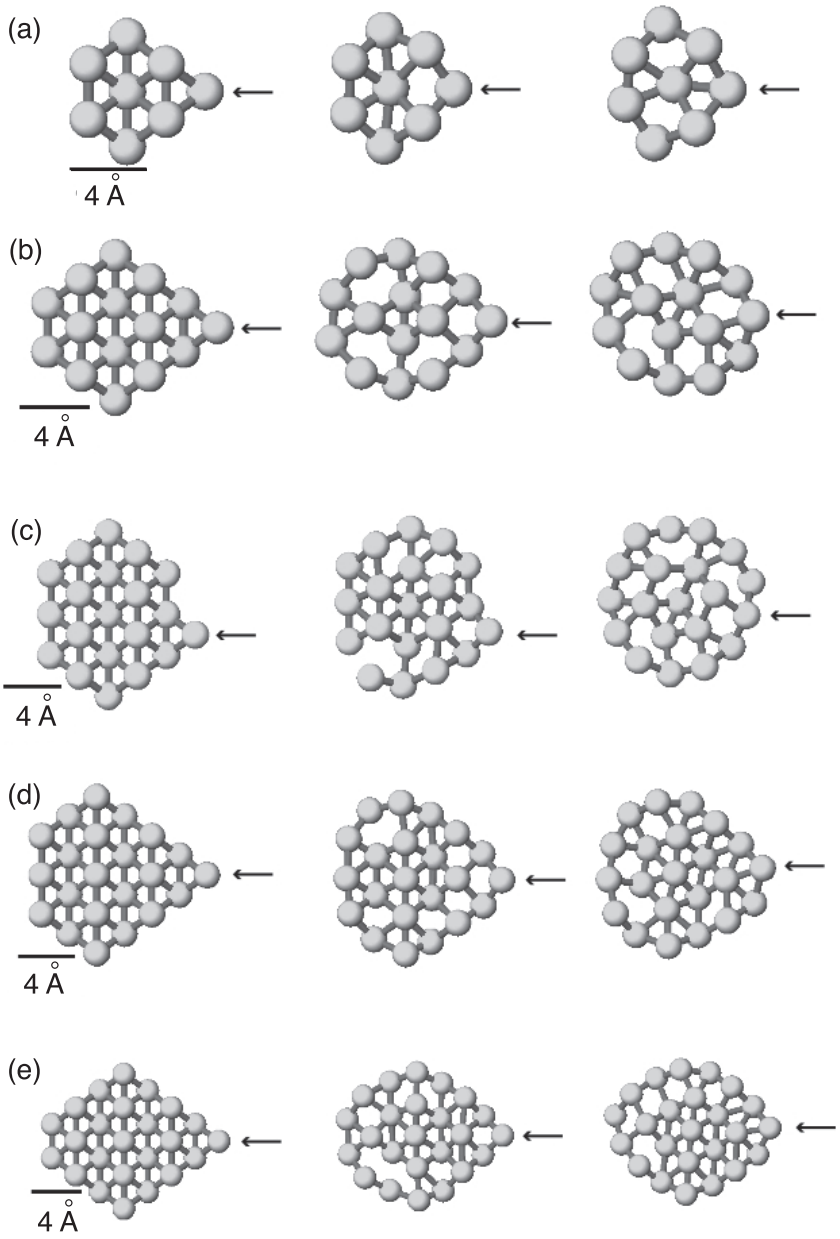

FIG. 10: Section views in relaxation process of the gold nanowires into helical structures; (a) 7-1 structure at the initial (left), 400-th (middle) and 5,000-th iteration steps (right), (b) 11-4 structure at the initial (left), 400-th (middle) and 6,000-th iteration steps (right), (c) 13-6-1 structure at the initial (left), 750-th (middle) and 9,000-th iteration steps (right), (d) 14-7-1 structure at the initial (left), 400-th (middle) and 7,000-th iteration steps (right), and (e) 15-8-1 structure at the initial (left), 400-th (middle) and 5,000-th iteration steps (right). An atom row is marked by arrow for each system. See text for details.

appear in all cases except the 12-6-1 nanowire at 600 K. The results shown in Fig. 10 are those at T=600K for (a),(b) (c) and (e) and at T=900K for (d).

As a typical case, Figs. 11(a)-(d) shows a set of sideviews in the case of the 11-4 structure at T=600K. Figures 11 (a)-(d) indicates that the square tiles on the (001)-type surface at the initial structure are transformed into the hexagonal (111)-type surface, as in Fig. 9 (c) and (d). The transformation propagates from the top and bottom of

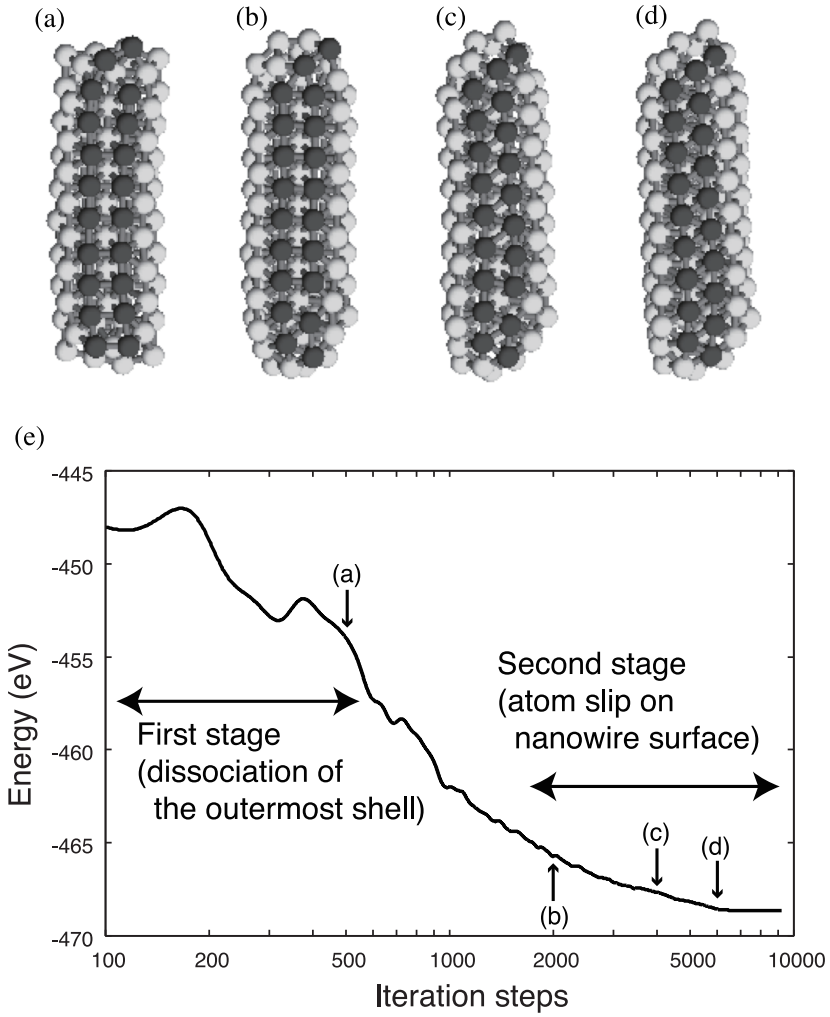

FIG. 11: Formation of helical 11-4 gold nanowire in relaxation process. Sideviews at the (a) 500-th, (b) 2000-th, (c) 4000-th and (d) 6000-th iteration step. Dark atoms are those that are placed initially on the (001)-type (square) surface and are transformed into a (111)-type (hexagonal) surface. (e) Change of the energy during the formation process. The iteration steps of (a) (b) (c) and (d) are indicated by arrows.

the nanowire. In the snapshot of Fig. 11(c), for example, the transformation has been completed except the region near the third lowest layer and the transformation. The energy of the nanowire is plotted in Fig. 11(e) as the function of iteration step and decreases almost monotonically after the 1,000-th iteration step.

It should be noted that the present simulation is different from experiment in several points. For example, the time scale of the process is quite short, on the order of 10 ps, owing to the practical limit of computational resource. Therefore, the simulation result should be understood so that it captures an intrinsic energetical mechanism of the real process.

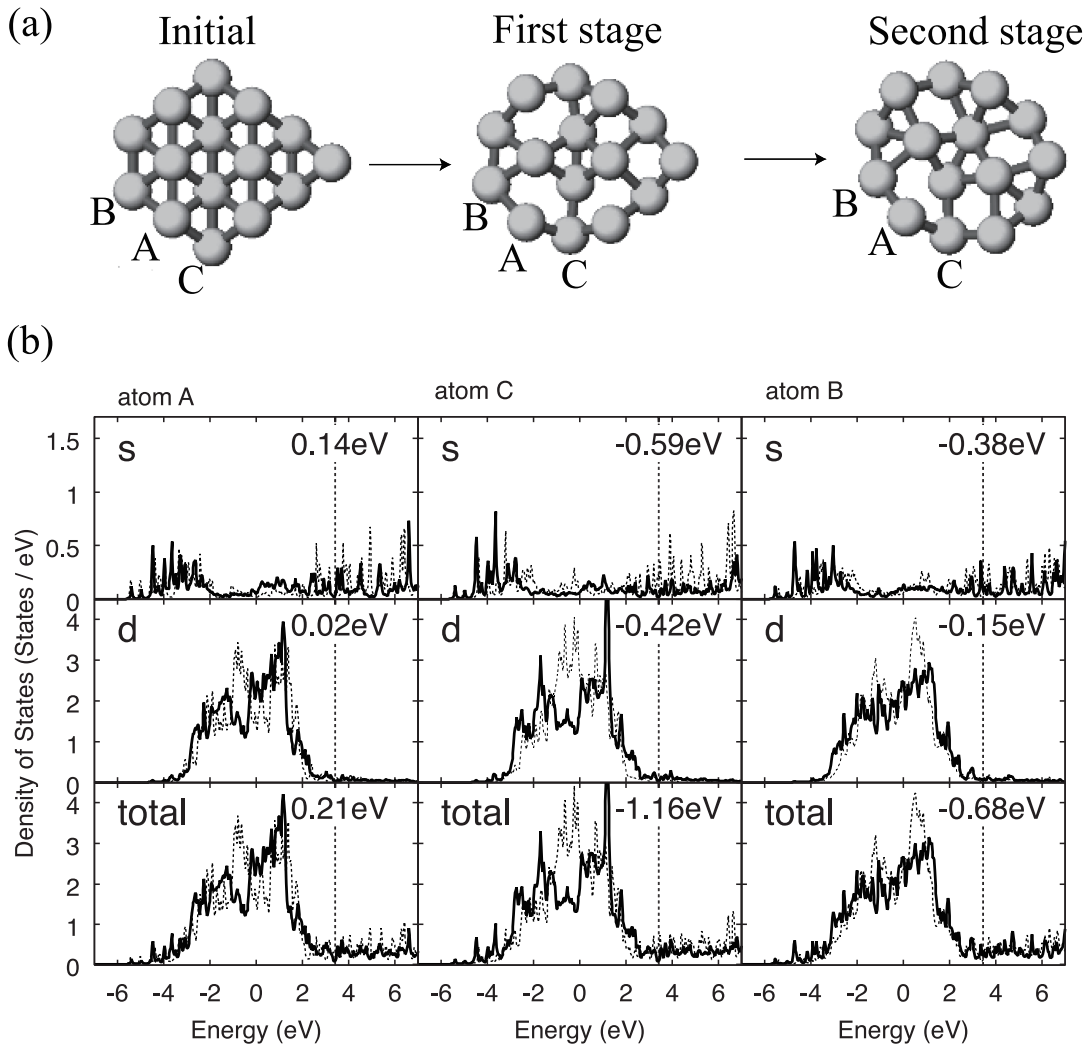

FIG. 12: Analysis of the two stage formation process in the 11-4 gold helical nanowire. (a) The section views with specifying the atoms A, B and C. The snapshots are the same as those in Fig. 10(b). (b) Local density of states of the atoms A, C and B at different iteration steps. The solid and broken lines in (b) are at the initial state and at the 500-th iteration step respectively for the atoms A and C, and at the 500-th and 5,000-th steps for the atom B. The difference of the local energy between the two iteration steps is written at the right corner of each panel. The vertical broken line indicates the Fermi level. The upper, middle, and lower panels of (b) are the partial densities of states of s orbital, d orbital, and the total density of states, respectively. In each panel, the difference of the local energy between the two iteration steps is written at the upper right corner of each panel.

D. Analysis of electronic structure

The mechanism of the two stage formation process is investigated by analyzing local electronic structure. A typical case of the 11-4 structure with $T = 600$K is picked out for explanation.

Local density of states (LDOS) and 'local energy' are used throughout the analysis. In general, LDOS is defined for each atom and can be decomposed into the contributions

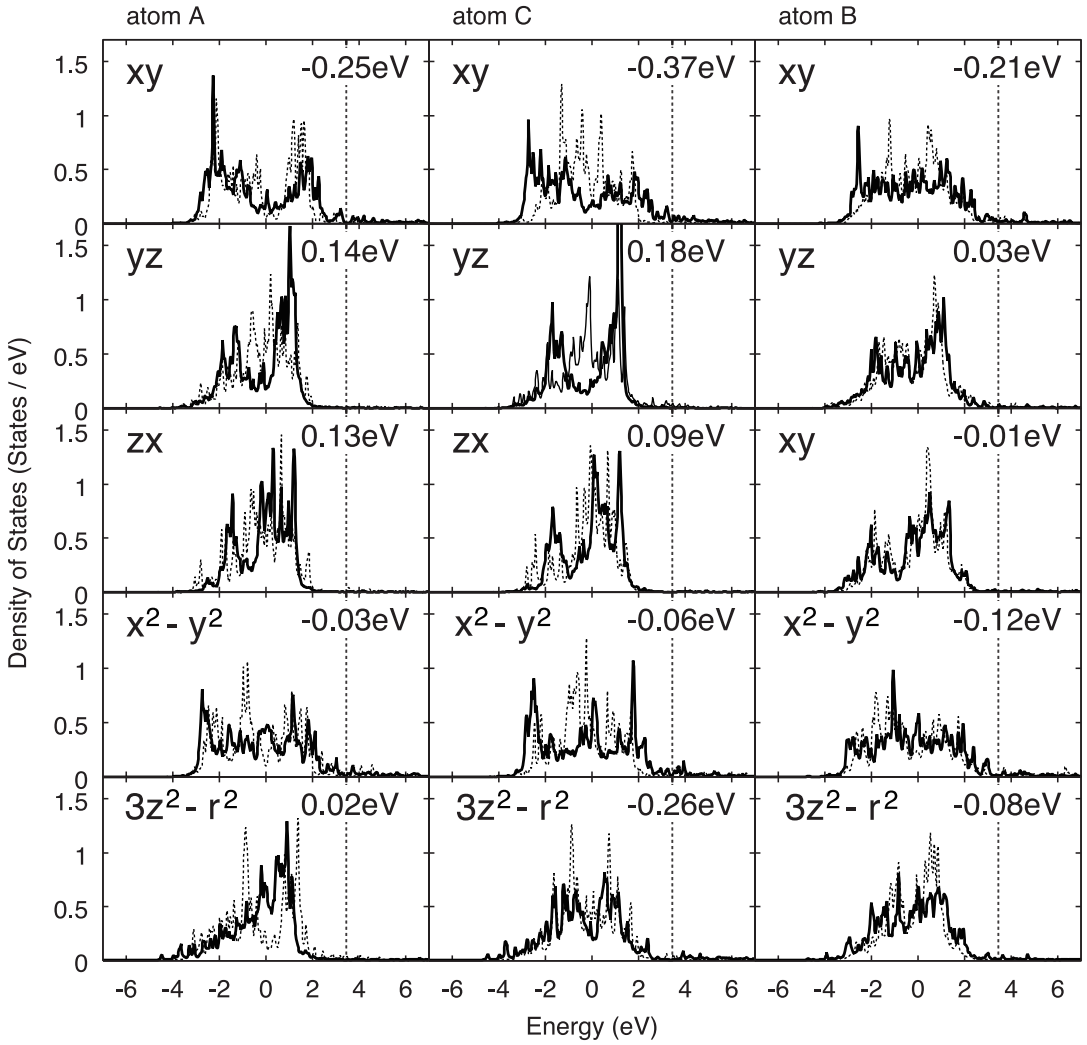

FIG. 13: LDOS for each d orbital of the atoms A, C and B at the two iteration steps in the relaxation process of the 11-4 gold nanowire. The definitions and notations are the same as in Fig. 12. Local coordinate system for each atom is written in text.

of each orbital. The profile of LDOS means the energy spectrum of electronic states at a local region near the atom. 'Local energy' is defined for each atom or orbital by the energy integration of LDOS within the occupied energy region. A decrease of the local energy during the process means that the atom gains the energy by a binding mechanism.

Fig. 12 shows local density of states (LDOS) of specific atoms at specific iteration steps. The section views of Fig. 12(a) are identical to those of Fig. 10(b). The LDOS for the atoms A, B and C in Fig. 12(a) are plotted in Fig. 12(b). The solid and broken lines are the LDOS profile at the initial and 500-th steps for the atoms A and C, and are at the 500-th and 5,000-th steps for the atom B, respectively. The vertical broken line indicates the Fermi level and the positions of the Fermi level are almost the same in the two iteration steps and indistinguishable in the graphs. The top panel of Fig. 12(b) is the LDOS for the s orbital and the middle panel is the LDOS for the d orbitals. The p

orbitals are also included in the simulation but their contribution in the energy range of Fig. 12(b) is small. The bottom panel is the total LDOS value that is contributed by the s, p and d orbitals. In each panel of Fig. 12(b), the difference of the local energy between the two iteration steps is written at the upper right corner. A negative or positive value of the difference means an energy gain or loss during the process, respectively.

The LDOS for each d orbital is also plotted Fig. 13, which will be key for understanding the mechanism. The shape of the d orbitals are shown in Fig. 2 Here a local coordinate system is defined for each atom as follows; The local x-axis is the nanowire axis, [110], the local y-axis is along the lateral direction and the local z-axis is perpendicular to the surface. Therefore, the wire surface corresponds to the xy plane at each atom.

The first stage of the process can be explained by the change of LDOS of the atoms A and C. Figure 12 indicates that the dissociation of the atom A occurs with an energy loss by 0.21 eV, because of the reduction of its coordination number. It is remarkable, however, that the energy loss of the d electrons is quite small (0.02eV), when it is compared with that of the s electron (0.14 eV). Here one should remember that the number of d electrons is larger, by about ten times, than that of s electrons ($d^{10}s^1$). The left column of Fig. 13, the data of the d orbitals at the atom A, indicates that the energy gain and loss among the d orbitals are on the order of 0.1 eV but they cancel with each other. The energy gain or loss mechanism of each orbital can be explained by the spatial spread of each orbital; The local energy of the yz orbital of the atom A increases, since the orbital extents perpendicularly to the wire surface and the nearest neighbor distance increases. The local energy of the xy orbital decreases, since the orbital can expand more to another (111)-type sheet through the atom C because of flattening two (111)-type sheets and the band width becomes wider.

It is also remarkable in Fig. 12 that the atom C has a large energy gain, by 1.16 eV, at the first stage. The middle column of Fig. 13 indicates that the largest energy gain comes from that of the xy orbital (0.37eV). Therefore, the local energy of the d orbitals decreases on the atom C. This energy gain of d orbitals can be attributed to the flattened surface structure around the atom C after the dissociation between the atom A and the inner shell. The energy of s orbital of the atom C also decreases appreciably but it may be not associated primarily with the dissociation, since the s orbital does not always favor the flatter atomic configurations.

The second stage is explained by the change of LDOS of the atom B. The local energy of the s orbital decreases by 0.38 eV (Fig. 12(b)), since the coordination number

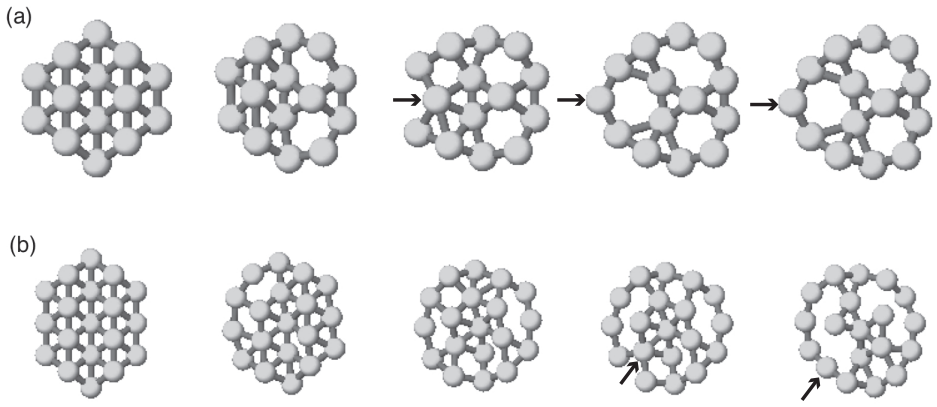

FIG. 14: Relaxation process of the (a)10-4 and (b) 12-6-1 gold nanowires into helical structures. The panels of (a), from right to left, are the snapshots at every 500 step from the initial one and the panels of (b) are those at every 2500 step from the initial one. An atom marked by arrow indicates the atom row that moves from an inner shell into the outermost one.

of the atom B increases like an atom depicted by filled square in Figs. 9(c) and (d). The local energy of the d orbital of the atom B also decreases by 0.15 eV (Fig. 12(b)). In particular, the xy orbital gives the largest energy gain among the d orbitals, by 0.21 eV (Fig. 13)), since the surface transforms to (111)-type and is flattened. Here, the slip deformation is essential since it widens the area of the (111)-like hexagonal surface and the LDOS of the xy orbital transfers its weight from the anti-bonding region (the high energy region) to the bonding region (the low energy region) (Fig. 12). Here one should recall that the atom A is connected with the atom B and can move relatively freely from the inner shell, after the dissociation at the first stage. Therefore, the atom B slips easily and introduces the helicity, since the atom B can trail other atoms without dissociating their bonds.

The above analysis is concluded that the first and second stages are governed by the energy gain mechanism of d orbitals among atoms on or near the (001)-type surface area. If a wire has a larger diameter than those in this section, the ratio of the energy gain to the total energy will be smaller and the transformation will not occur.

E. Discussions

Three points are discussed for the two stage formation model.

First, the 10-4 and 12-6-1 nanowires are discussed. They are ones of the 'reference' structures (See Fig. 8) and do not have an additional atom row on the outermost shell unlike the nanowires in Fig. 10. Figure 14 shows relaxation process of the 10-4 nanowire at $T = 600K$ and the 12-6-1 nanowires at $T = 900K$. These nanowires are transformed

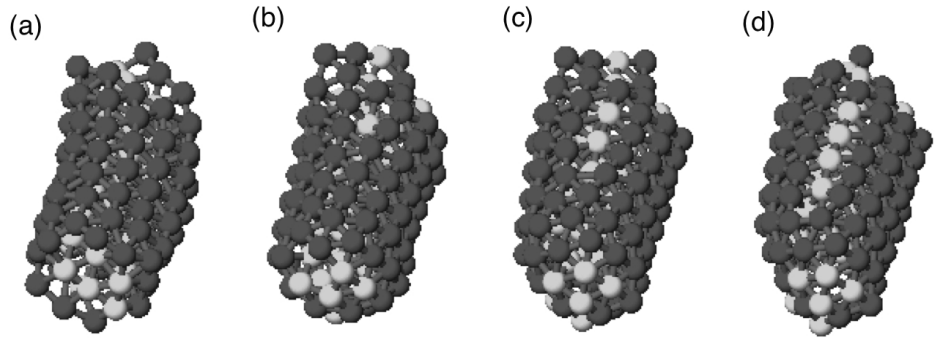

FIG. 15: Relaxation process of 12-6-1 gold nanowire into helical structures; (a) 750-th, (b) 5000-th, (c) 9500-th and (d)14500-th iteration steps. The atoms in the outer and inner shells are shown as dark and light balls, respectively.

into helical ones. In the transformation process, an atom row indicated by arrows in Fig. 14 (a) or (b) moves from the inner shell into the outermost one, unlike the cases in Fig. 10. The final snapshots in Fig. 14 (a) and (b) are the helical 11-3 and 13-5-1 (or 13-6) structures, respectively. Figure 15 shows the transformation process of the 12-6-1 case from a different viewpoint, so as to clarify the atom row movement.

The two stage formation model holds also in these nanowires. The present results show that the inserted atom rows are supplied possibly from outer and inner regions. For example, in the 13-6-1 nanowire (See Fig.10(c)), an atom row is supplied from the outer region into the shell with twelve atoms, while, in the 12-6-1 nanowire (See Fig. 14(b)), an atom row is supplied from the inner region into the shell with twelve atoms. Both nanowires show surface reconstruction into helical structure with the outermost shell of thirteen atoms.

Second, QM-MD simulation for copper nanowire was carried out for comparison with gold nanowires. The calculation of the copper 11-4 nanowire was simulated and temperature was set to be 600 and 900 K, which is lower than the melting temperature (1358K). As result, helical wire appeared at 900 K but did not at 600 K, since the surface atom did not dissociate from the inner shell at 600K. These results lead us to the conclusion that copper nanowire is more difficult than gold one to be transformed into helical structure, which is consistent to the fact that no helical copper nanowire was observed in experiment.

Local electronic structure is analyzed in the 11-4 copper nanowire at $T = 600$K. Figure 16 shows the LDOS calculations for the atoms A, C at the initial structure and the 500-th iteration step. The definitions and notations are the same as in the gold case (Fig. 12(b)). The two vertical broken lines are the values of the Fermi level at the two

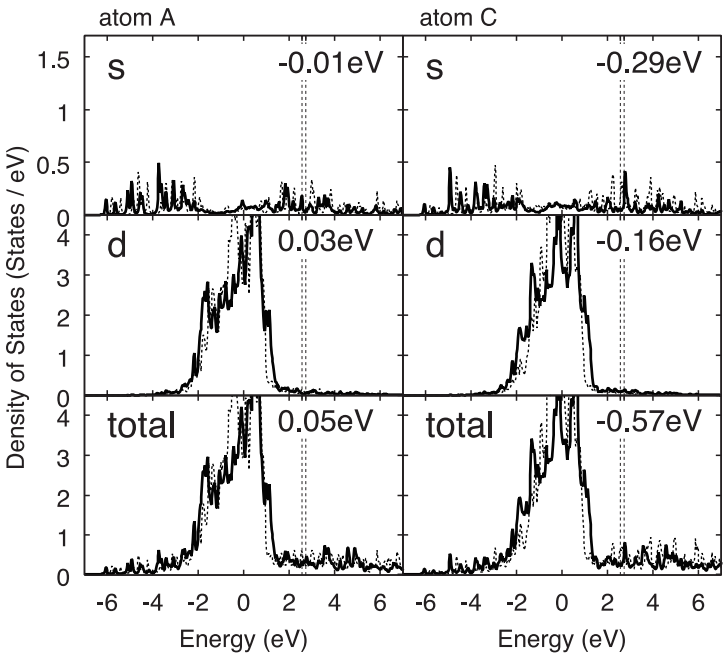

FIG. 16: Local density of states in the 11-4 copper nanowire for the atoms A and C. The solid and broken lines are at the initial state and at the 500-th iteration step, respectively. The difference of the local energy between the two iteration steps is written at the right corner of each panel. The definitions and notations are the same as in Fig. 12(b).

iterations and the higher value is that at the 500-th iteration step. Figure 17 shows LDOS for each d orbital of the atoms A, C at the two iteration steps. The definitions and notations are the same as in Fig. 13. As common features of the LDOS of copper nanowire (Figs. 16 and 17) and gold nanowire (Fig. 12(b) and Fig. 13), the energy gain of d orbitals at the atom C is seen and the maximum energy gain is given by the xy orbital among d orbitals.

The theory in the previous sections explains the above results; Copper, silver and gold have ten d electrons ($d^{10}s^1$) but the d band width of gold is wider than that of copper and silver (See Fig. 5). Therefore, the energy gain mechanism for helical transformation is inherent in copper but its effect is weaker than that in gold. This is why helical structure appears in gold nanowire but not in copper nanowire.

The above theory also explains why platinum helical nanowire can be formed, since platinum and gold has the $5d$ band (See Fig. 1(b)) which is wider than the $3d$ and $4d$ band in the lighter elements of Fig. 1(b). The energy gain mechanism in the two stage formation model is governed by the d band width and the helical nanowires appear only among metals with a wider d band.

Third, the similarity in mechanism is discussed between helical nanowires and equilibrium surfaces. Since the present mechanism is based on the electronic structure of $5d$

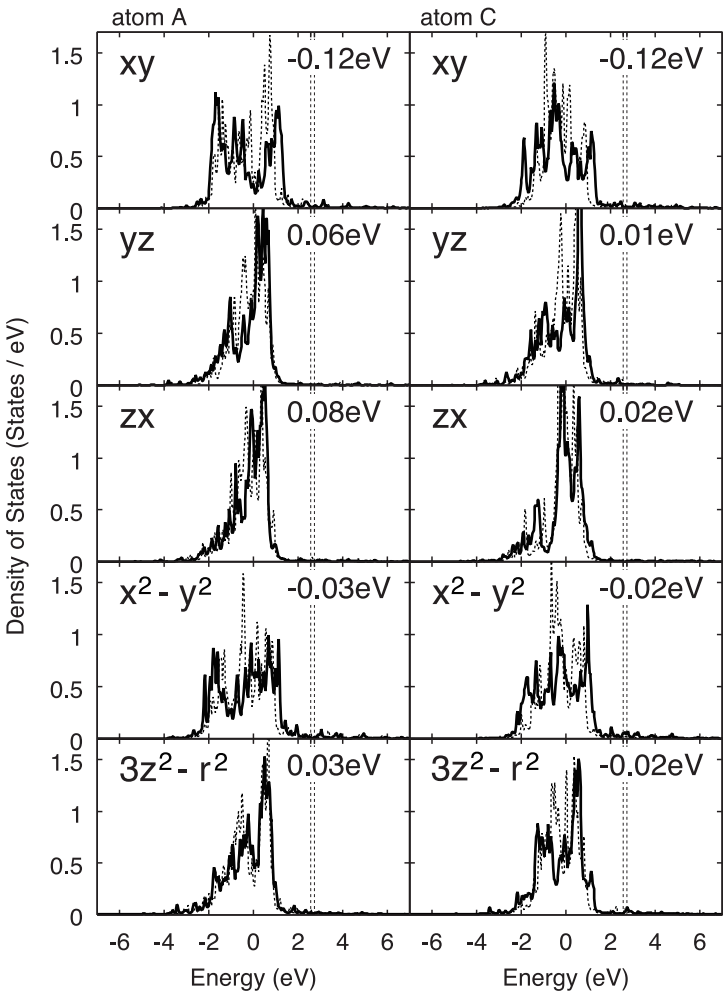

FIG. 17: LDOS for each d orbital of the atoms A, C at the two iteration steps in the relaxation process of the 11-4 copper nanowire. The solid and broken lines are at the initial state and at the 500-th iteration step, respectively. The definitions and notations are the same as in Fig. 13.

band, the mechanism is inherent not only with nanowires but also with bulk surfaces of FCC $5d$ metals, gold, platinum and iridium (Ir) (See Fig.1(b)). For example, the equilibrium (110) surfaces of these elements reconstruct into a 2×1 'missing row' structure, [Fedak *et al.* 1967, Binnig *et al.* 1983, Ho and Bohnen 1987] in which (111)-type hexagonal surfaces appear as successive nanofacets.

Figure 18(a) and (b) shows the top and side views of the missing row structure. The cubic cell of the ideal FCC structure, identical to Fig. 3(a), is also shown in Fig. 18(c) for tutorial. The (110)-2×1 missing row structure appears, when one removes every other row in the [001] direction from the ideal (110) surface. The atom position of missing rows are drawn by the crosses in Fig. 18(b). In the ideal FCC structure of Fig. 18(c), the ideal (110) surface corresponds to the plane with the atoms R, P, S and U. The atom positions of the 'missing row' are those on the atom row that contains the atoms S and U. In Figs. 18(a) and (b), (111)-type facets appears, such as one that contains

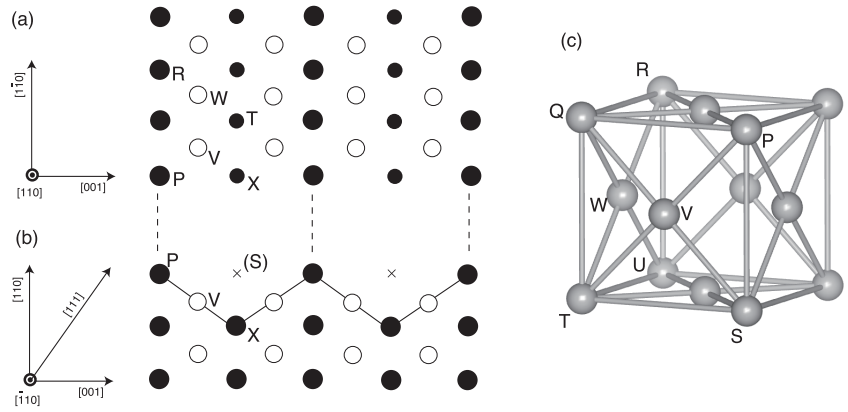

FIG. 18: (a) Top and (b) side views of the 'missing row' structure in FCC(110) surface. (c) Ideal FCC structure. In (a), three successive atomic layers are drawn. Atoms are distinguished by larger filled circles, open circles or smaller filled circles, for the first, second, third surface layers, respectively. In (b), two successive atomic layers are drawn. Atoms are distinguished by filled and open circles. The crosses in (b) indicates the site of the 'missing row'. The lines in (b) indicate (111)-type surface regions as successive nanofacets. The atoms marked as P, R, R, S, T, U, V and W appear among (a)-(c). The atom marked X appears only in (a) and (b).

the atoms P, V, T, W and R. One can confirm in Figs. 18(c) that the atoms P, V, T, W and R are on a (111)-type plane.

Moreover, the equilibrium (001) surfaces of these elements also show reconstruction in which a surface layer with (111)-type hexagonal regions is placed on the (001)-type square layers. [Van Hove *et al.* 1981, Binnig *et al.* 1984, Abernathy *et al.* 1992, Jahns *et al.* 1999]

It should be noted that, an experimental paper of [110] gold nanowire [Kondo and Takayanagi 1997], earlier than the report of helical structure[Kondo and Takayanagi 2000], suggests that (001)-type regions on the nanowire surface reconstruct into (111)-type ones, as on equilibrium surfaces. The suggested reconstruction mechanism is consistent to the present one.

V. SUMMARY AND FUTURE ASPECT

This article gives a review of ultrathin gold nanowire and focuses two properties; (i) monoatomic chain with quantized conductance and (ii) helical multishell structures with 'magic numbers'. The first property is general among different metal nanowires. The second property is unique for gold and platinum. The proposed theory with two stage formation process and analysis of electronic structure explains how and why these helical structures appear. The appearance of helical multishell gold nanowire should be

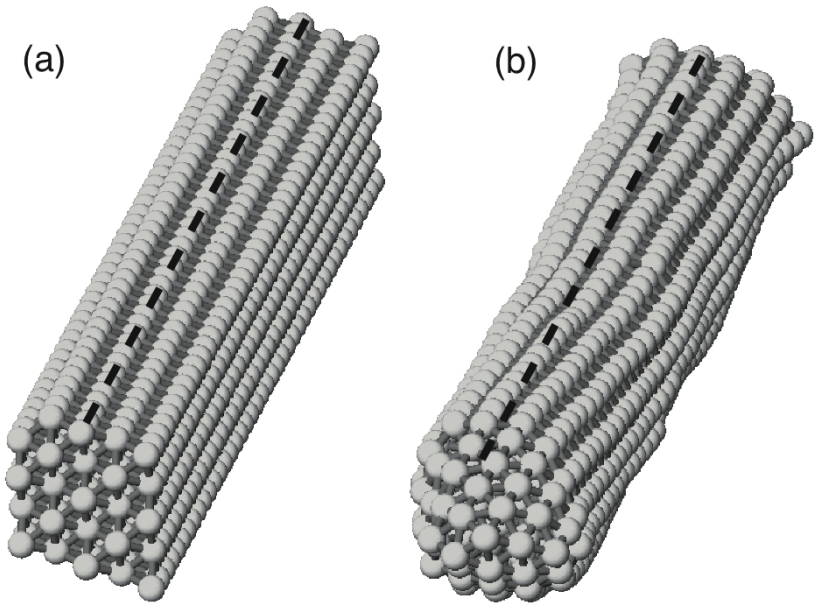

FIG. 19: Transformation of 15-8-1 helical structure of a gold nanowire with the length of 12 nm. Initial (left) and final (right) snapshots are shown. A dashed line is drawn for an eye guide commonly on the two snapshots.

understood by the following two points; (i) This is a typical nanoscale effect, in which the numbers of atoms in surface (outermost) region and bulk (inner) region are comparable and the structure is determined by the energy gain mechanism of the surface region. (ii) This is a typical quantum mechanical effect, in which the electronic structure, the non-spherical property of $5d$ band, governs the phenomena.

As a future aspect, structural and transport properties should be investigated further for 'thicker' nanowire, so as to establish the foundation of nano electronics. The investigation of helical multishell nanowires is typical one and other investigations were explained in Sec. III. The above two points should be of general importance among the investigations of 'thicker' nanowires. Moreover, 'thicker' nanowires can show complex transport property, since the interference of electron 'wave' is influenced by the structures of nanowire and electrodes and the character of valence orbitals. Among such cases, the conductance value is, in general, not quantized and a more fundamental expression of Eq. (4) should be considered. An example is found in theoretical [Ono and Hirose 2005] and experimental [Oshima *et al.* 2006] papers of helical multishell gold nanowires. The papers point out that the structure of electrode parts varies conductance value. For another example, transport behavior was investigated for model 'thicker' nanowires. [Shinaoka *et al.* 2008] The paper focuses on electrode effect and d orbital effect on conductance and local current.

Theoretical investigation of 'thicker' nanowire requires quantum-mechanical simulation with a larger number of atoms. For an example,[Fujiwara *et al.* 2008] Fig. 19 shows a simulation of a 15-8-1 nanowire with the wire length of 12 nm. The number of atoms is 1020. The resultant nanowire contains multiple helical domains on wire surface with well-defined domain boundary, which cannot be obtained in smaller samples. More systematic investigations will be given in near future. When one would like to compare simulations with experiment, the above system size is still insufficient and electrode parts are missing in the simulation. A promising theoretical approach for larger quantum-mechanical simulations is 'order-N' method, in which the computational time is 'order-N' or proportional to the system size N. See articles cited in Ref.[Hoshi and Fujiwara 2006] or a recent journal volume that includes Ref. [Fujiwara *et al.* 2008] and focuses on the order-N methods.

APPENDIX A: NOTE ON QUANTUM-MECHANICAL MOLECULAR DYNAMICS SIMULATION

This note is devoted to a tutorial of QM-MD simulation. See a textbook [Martin 2004] for general introduction of quantum mechanical (electronic structure) calculations. QM-MD simulation method is based on quantum mechanical description of electrons and classical description of atomic nuclei. Atomic structure is determined with the electronic wavefunctions. Since the mass of atomic nucleus is heavier by more than 1000 times than that of electron, the motion of atomic nucleus is treated adiabatically. In many QM-MD simulations, only valence electrons are treated explicitly and nucleus and core electrons are treated as 'ions'.

Electronic wave functions are determined with given position of the atomic nuclei or ions $\{\boldsymbol{R}_I\}$ and the effective Schrödinger equation is obtained as

$$H\phi_i = \varepsilon_i \phi_i, \tag{A1}$$

where H is an effective Hamiltonian and $\phi_i \equiv \phi_i(\boldsymbol{r})$ and ε_i are electronic wavefunction and its energy level, respectively. The motion of atomic nuclei or ions is described by their position $\{\boldsymbol{R}_I\}$ and velocity $\{\boldsymbol{V}_I\}$ and the Newton equation is derived

$$M_I \frac{d\boldsymbol{V}_I}{dt} = \boldsymbol{F}_I, \tag{A2}$$

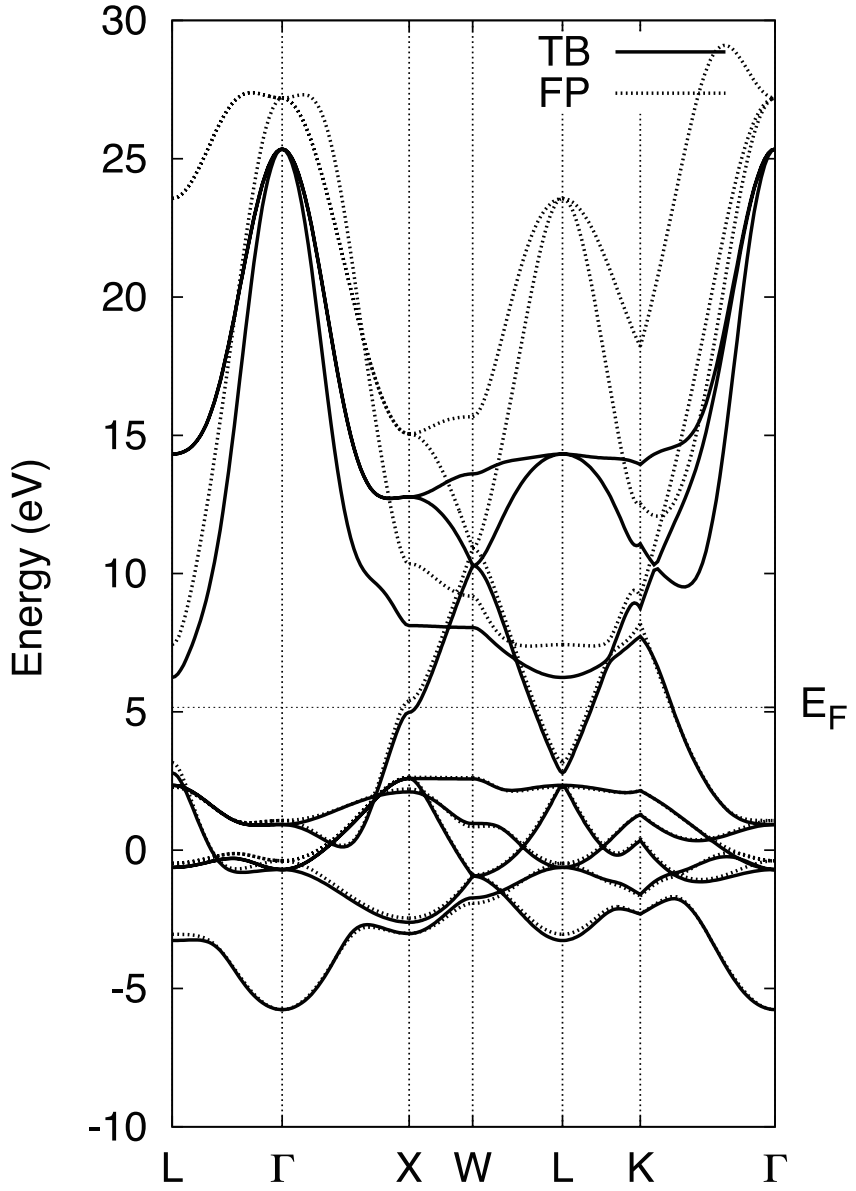

FIG. 20: Band diagrams of bulk gold that are calculated by the tight-binding form Hamiltonian (TB) and the first-principles one (FP). See text for details.

where the force $\boldsymbol{F}_I$ is given by the derivative of the energy $E[\{\boldsymbol{R}_I\}]$;

$$\boldsymbol{F}_I = -\frac{\partial E}{\partial \boldsymbol{R}_I}. \tag{A3}$$

The energy $E[\{\boldsymbol{R}_I\}]$ and the force $\{\boldsymbol{F}_I\}$ depend on the solutions $\{\phi_i(\boldsymbol{r})\}$ of Eq. (A1). A well-established method in QM-MD simulation is the first principles molecular dynamics that is realized by plane-wave bases and density functional theory. [Martin 2004, Car and Parrinello 1985, Payne *et al.* 1992]

The procedure of QM-MD simulation within one time step is summarized as

$$\{\mathbf{R}_I\} \Rightarrow \{\varepsilon_i, \phi_i(\boldsymbol{r})\} \Rightarrow E, \{\boldsymbol{F}_I\} \Rightarrow \text{update}\,\{\mathbf{R}_I\}; \tag{A4}$$

(i) With given positions $\{\boldsymbol{R}_I\}$, the effective Schrödinger equation of Eq. (A1) is solved and the energy levels and wavefunctions for electrons ($\{\varepsilon_i, \phi_i(\boldsymbol{r})\}$) are obtained. (ii) The total energy E and the forces $\{\boldsymbol{F}_I\}$ are obtained. (iii) The positions are updated ($\boldsymbol{R}_I(t) \Rightarrow \boldsymbol{R}_I(t+\delta t)$) by a numerical time evolution of Eq. (A2) with a tiny time interval δt. The time interval δt is usually on the order of femto second.

The QM-MD simulation shown in Sec. IV was realized by the simulation code 'ELSES' (=Extra-Large-Scale Electronic Structure calculations). See the web page (http://www.elses.jp/) or the papers [Hoshi and Fujiwara 2000, Hoshi and Fujiwara 2003, Geshi *et al.* 2004, Takayama *et al.* 2004, Hoshi *et al.* 2005, Takayama *et al.* 2006, Hoshi and Fujiwara 2006, Iguchi *et al.* 2007, Fujiwara *et al.* 2008, Hoshi and Fujiwara 2009]. In the simulation, Slater-Koster or tight-binding form Hamiltonian is used. In general, a QM-MD simulation with tight-binding form Hamiltonians enable a much faster simulation than the first principles molecular dynamics, although it has not yet established to construct tight-binding form Hamiltonians among general materials from the first principles.

In the simulations of gold and copper in Sec. IV, the energy $E[\{\boldsymbol{R}_I\}]$ and the Hamiltonian H are written within the tight-binding form developed in Naval Research Laboratory [Mehl and Papaconstantopoulos 1996, Kirchhoff *et al.* 2001, Papaconstantopoulos and Mehl 2003, Haftel *et al.* 2004]. The form contains several parameters and they are determined to represent electronic structures of bulk solids, surfaces, stacking faults and point defects. Gold nanowires were calculated by the present Hamiltonian. [da Silva *et al.* 2001, da Silva *et al.* 2004, Haftel and Gall 2006, Iguchi *et al.* 2007]

Figure 20 shows the energy band diagrams of FCC gold calculated by the present tight-binding form Hamiltonian and the first-principles one with linear muffin-tin orbital theory [Andersen and Jepsen 1984]. In general, the energy band diagram is a standard method for visualizing electronic state in solid. The diagram describes the relation between energy ε and wavevector $\boldsymbol{k}$ of electronic states ($\varepsilon = \varepsilon(\boldsymbol{k})$). Each point in the horizontal axis indicates a wavevector $\boldsymbol{k}$. Several specific wavevectors are labelled, such as 'Γ'. See a textbook [Bradley and Cracknell 1972] for their definitions. In Fig. 20, the energy band diagram by the tight-binding form Hamiltonian reproduces well that by the

first-principles Hamiltonian, particularly in the occupied energy region ($E < E_{\rm F}$). The electronic structure in the occupied energy region contributes to the cohesive mechanism and determines atomic structures.

Tight-binding form Hamiltonians for QM-MD simulation were developed also by many other groups, which can be found, for example, in a review paper [Goringe *et al.* 1997]. Some of them are developed for specific elements, such as ones for C [Xu *et al.* 1992] and Si [Kwon *et al.* 1994] and some of them, Refs. [Calzaferri *et al.* 1989, Calzaferri and Rytz 1996, Nath and Anderson 1990] for example, were developed for more general materials.

Analysis method of electronic wavefunction is also important for understanding phenomena. A bond between two atoms can be determined by electronic wavefunction through the theory of crystal orbital Hamiltonian population (COHP) [Dronskowski and Blöchl 1993], a well-defined energy spectrum of bond. In Sec. IV, the dissociation of two atoms was ascertained in two ways; (1) the interatomic distance increases by more than 20 % and (2) the peak height of the COHP decreases down to 1/5 of that of the initial state.

[Abernathy *et al.* 1992] Abernathy, D. L., S. G. J. Mochrie, D. M. Zehner, G. Grübel and D. Gibbs. 1992. Orientational epitaxy and lateral structure of the hexagonally reconstructed Pt(001) and Au(001) surfaces. Phys. Rev. B **45**: 9272-9291.

[Agraït *et al.* 1993] Agraït, N. J. G. Rodrigo and S. Vieira, 1993. Conductance steps and quantization in atomic-size contacts. Phys. Rev. B **47**: 12345-12348.

[Agraït *et al.* 2003] Agraït, N., A. L. Yeyati and .J. M. van Ruitenbeek. 2003. Quantum properties of atomic-sized conductors. Phys. Rep. **377**: 81-279.

[Amorim *et al.* 2008] Amorim, E. P. M. and E. Z. da Silva. 2008. Helical [110] Gold Nanowires Make Longer Linear Atomic Chains. Phys. Rev. Lett. **101**: 125502 (4pp).

[Andersen and Jepsen 1984] Andersen, O. K. and O. Jepsen, 1984. Explicit, first-principles tight-binding theory. Phys. Rev. Lett. **53** : 2571-2574

[Bettini *et al.* 2005] Bettini, J., V. Rodrigues, J. C. González and D. Ugarte. 2005. Real-time atomic resolution study of metal nanowires Appl. Phys. A**81**: 1513-1518.

[Bilalbegović 2003] Bilalbegović, G. 2003. Gold nanotube: structure and melting. Vacuum **71**: 165-169.

[Binnig *et al.* 1983] Binnig, G., H. Rohrer, Ch. Gerber and E. Weibel. 1983. (111) facets as

the origin of reconstructed Au(110) surfaces. Surf. Sci, **131**:L379-L384.

[Binnig *et al.* 1984] Binnig, G.K., H. Rohrer, Ch. Gerber and E. Stoll. 1984. Real-space observation of the reconstruction of Au(100). Surf. Sci. **144**: 321-335.

[Bradley and Cracknell 1972] Bradley C. J. and A. P. Cracknell. 1972. *The Mathematical Theory of Symmetry in Solids*, Clarendon Press, Oxford.

[Brandbyge *et al.* 1999] Brandbyge, M., N. Kobayashi, and M. Tsukada. 1999. Conduction channels at Fnite bias in single-atom gold contacts. Phys. Rev. B **60**:17064-17070.

[Brandbyge *et al.* 1985] Brandbyge, M., J. Schiøtz, M. R. Sørensen, P. Stoltze, K. W. Jacobsen, J. K. Nørskov, L. Olesen, E. Laegsgaard, I. Stensgaard, and F. Besenbacher. 1985. Quantized conductance in atom-sized wires between two metals. Phys. Rev. B **52**: 8499-8514.

[Calzaferri *et al.* 1989] Calzaferri, G., L. Forss, and I. Kamber. 1989. Molecular geometries by the extended Hückel molecular orbital method. J. Phys. Chem. **93**: 5366.

[Calzaferri and Rytz 1996] Calzaferri G. and R. Rytz. 1996. The band structure of diamond. J. Phys. Chem. **100**:11122.

[Car and Parrinello 1985] Car, R. and M. Parrinello. 1985. Unified approach for molecular dynamics and density-functional theory. Phys. Rev. Lett. 55: 2471-2474.

[Costa-Krämer *et al.* 1997] Costa-Krämer, J. L., N. García and H. Olin. 1997. Conductance quantization histograms of gold nanowires at 4 K. Phys. Rev. B **55**: 12910-12913.

[Cuevas *et al.* 1998] Cuevas, J. C., A. Levy Yeyati, and A. Martin-Rodero. 1998. Microscopic origin of conducting channels in metallic atomic-size contacts. Phys. Rev. Lett. **80**: 1066-1069.

[da Silva *et al.* 2001] da Silva, E. Z., da Silva, A. J. R., and Fazzio, A. 2001. How do gold wires break ? Phys. Rev. Lett. **87**: 256102. (4pp).

[da Silva *et al.* 2004] da Silva, E. Z., F. D. Novaes, A. J. R. da Silva and Fazzio, A. 2004. Theoretical study of the formation, evolution, and breaking of gold nanowires. Phys. Rev. B **69**:115411 (11pp).

[Datta 1995] Datta, S. 1995. *Electronics Transport in Mesoscopic Systems*, Cambridge University Press, Cambridge.

[Dresselhaus *et al.* 2001] Dresselhaus, M. S., G. Dresselhaus, P. Avouris, Ed. 2001. *Carbon Nanotubes - Synthesis, Structure, Properties, and Applications*, Springer, Berlin

[Dronskowski and Blöchl 1993] Dronskowski, R. and P. E. Blöchl. 1993. Crystal orbital Hamilton populations (COHP). energy-resolved visualization of chemical bonding in solids based on density-functional calculations. J. Phys. Chem. **97**: 8617-8624.

[Erts *et al.* 2000] Erts, D., H. Olin, L. Ryen, E. Olsson and A. Thölén. 2000. Maxwell and Sharvin conductance in gold point contacts investigated using TEM-STM. Phys. Rev. B **61**: 12725-12727.

[Erts *et al.* 2002] Erts, D., A. Lõhmus, R. Lõhmus, H. Olin, A.V. Pokropivny, L. Ryen, K. Svensson. 2002. Force interactions and adhesion of gold contacts using a combined atomic force microscope and transmission electron microscope. Appl. Surf. Sci. **188**: 460-466.

[Fedak *et al.* 1967] Fedak D.G., and N.A. Gjostein. 1967. A low energy electron diffraction study of the (100), (110) and (111) surfaces of gold Acta Metal. **15**: 827-840.

[Fujiwara *et al.* 2008] Fujiwara, T., T. Hoshi and S. Yamamoto. 2008. Theory of large-scale matrix computation and applications to electronic structure calculation. J. Phys.: Condens. Matter **20**: 294202 (7pp).

[Fujimoto and Hirose 2003] Fujimoto, Y. and K. Hirose. 2003. First-principles treatments of electron transport properties for nanoscale junctions. Phys. Rev. B**67**: 195315 (12pp).

[Geshi *et al.* 2004] Geshi, M., T. Hoshi and T. Fujiwara. 2003. Million-atom molecular dynamics simulation by order-N electronic structure theory and parallel computation. J. Phys. Soc. Jpn. **72**:2880-2885.

[Goringe *et al.* 1997] Goringe, C. M., D. R. Bowler and E. Hernández. 1997. Tight-binding modelling for materials. Rep. Prog. Phys. **60**: 1447-1512.

[Gülseren *et al.* 1998] Gülseren, O., F. Ercolessi, E. Tosatti. 1998. Noncrystalline structures of ultrathin unsupported nanowires. Phys. Rev. Lett. **80**: 3775-3778.

[Haftel *et al.* 2004] Haftel, M.I., N. Bernstein, M. J. Mehl and D. A. Papaconstantopoulos. 2004. Interlayer surface relaxations and energies of fcc metal surfaces by a tight-binding method. Phys. Rev. B **70**: 125419 (15pp).

[Haftel and Gall 2006] Haftel, M. I. and K. Gall. 2006. Density functional theory investigation of surface-stress-induced phase transformations in fcc metal nanowires. Phys. Rev. B **74**: 035420 (12pp).

[Hansen *et al.* 1997] Hansen, K., E. Laegsgaard, I. Stensgaard, and F. Besenbacher. 1997. Quantized conductance in relays. Phys. Rev. B **56**: 2208-2220.

[Ho and Bohnen 1987] Ho, K.-M. and K. P. Bohnen. 1987. Stability of the missing-row reconstruction on fcc (110) transition metal surfaces. Phys. Rev. Lett. **59**: 1833-1836.

[Hoshi and Fujiwara 2000] Hoshi, T. and T. Fujiwara. 2000. Theory of composite-band Wannier states and order-N electronic-structure calculations. J. Phys. Soc. Jpn. **69**: 3773-3776.

[Hoshi and Fujiwara 2003] Hoshi, T. and T. Fujiwara. 2003. Dynamical brittle fractures of nanocrystalline silicon using large-scale electronic structure calculations. J. Phys. Soc. Jpn.

72:2429-2432.

[Hoshi and Fujiwara 2006] Hoshi, T. and T. Fujiwara. 2006. Large-scale electronic structure theory for simulating nanostructure processes. J. Phys: Condens. Matter. **18**:10787-10802.

[Hoshi and Fujiwara 2009] Hoshi, T. and T. Fujiwara. 2009. Development of the simulation package 'ELSES' for extra-large-scale electronic structure calculation J. Phys.: Condens. Matter **21**: 064233 (4pp).

[Hoshi *et al.* 2005] Hoshi, T., Y. Iguchi and T. Fujiwara. 2005. Nanoscale structures formed in silicon cleavage studied with large-scale electronic structure calculations: Surface reconstruction, steps, and bending. Phys. Rev. B**72**: 075323 (10pp).

[Iguchi 2007] Iguchi, Y. 2007. D. Thesis (in Japanese), Univ. of Tokyo, Tokyo.

[Iguchi *et al.* 2007] Iguchi, Y., T. Hoshi and T. Fujiwara. 2007. Two-Stage Formation Model and Helicity of Gold Nanowires. Phys. Rev. Lett. **99**: 125507 (4pp).

[Iijima 1991] Iijima, S. 1991. Helical microtubules of graphitic carbon. Nature **354** : 56-58.

[Jahns *et al.* 1999] Jahns, V., D. M. Zehner, G. M. Watson, D. Gibbs. 1999. Structure and phase behavior of the Ir(001) surface: X-ray scattering measurements. Surf. Sci, **430**: 55-66.

[Kirchhoff *et al.* 2001] Kirchhoff, F., M. J. Mehl, N. I. Papanicolaou, D. A. Papaconstantopoulos and F. S. Khan. 2001. Dynamical properties of Au from tight-binding molecular-dynamics simulations. Phys. Rev. B **63**: 195101 (7pp).

[Kizuka 1998] Kizuka, T. 1998. Atomic process of point contact in gold studied by time-resolved high-resolution transmission electron microscopy. Phys. Rev. Lett. **81** : 4448-4451.

[Kizuka 2007] Kizuka, T. 2007. Atomistic process of twin-boundary migration induced by shear deformation in gold. Jpn. J. Appl. Phys. **46**: 7396-7398.

[Kizuka 2008] Kizuka, T. 2008. Atomic configuration and mechanical and electrical properties of stable gold wires of single-atom width. Phys. Rev. B **77**: 155401 (11pp).

[Kizuka *et al.* 1997] Kizuka, T., K. Yamada, S. Deguchi, M. Naruse and N. Tanaka. 1997. Cross-sectional time-resolved high-resolution transmission electron microscopy of atomic-scale contact and noncontact-type scannings on gold surfaces. Phys. Rev. B 55: R7398-R7401

[Kizuka *et al.* 2001a] Kizuka, T., S. Umehara and S. Fujisawa. 2001. Metal-insulator transition in stable one-dimensional arrangements of single gold atoms. Jpn. J. Appl. Phys. **40**: L71-L74.

[Kizuka *et al.* 2001b] Kizuka, T., H. Ohmi. T. Sumi, K. Kumazawa, S. Deguchi, M. Naruse, S. Fujisawa, S. Sasaki, A. Yabe and Y. Enomoto. 2001. Simultaneous observation of millisecond

dynamics in atomistic structure, force and conductance on the basis of transmission electron microscopy. Jpn. J. Appl. Phys. **40**: L170-L173.

[Kondo and Takayanagi 1997] Kondo, Y. and K. Takayanagi. 1997. Gold nanobridge stabilized by surface structure. Phys. Rev. Lett. **79**: 3455-3458.

[Kondo and Takayanagi 2000] Kondo, Y, and K. Takayanagi 2000. Synthesis and characterization of helical multi-shell gold nanowires. Science **289** : 606-608.

[Krans *et al.* 1993] Krans, J. M., C. J. Muller, I. K. Yanson, Th. C. M. Govaert, R. Hesper and J. M. van Ruitenbeek. 1983. One-atom point contacts, Phys. Rev. B **48**: 14721-14724.

[Krans *et al.* 1995] Krans, J. M., J. M. van Ruitenbeek, V. V. Flsun, I. K. Yanson, L. J. de Jongh. 1995. The signature of conductance quantization in metallic point contacts. Nature **375**: 767-769.

[Kurui *et al.* 2007] Kurui, Y., Y. Oshima, M. Okamoto and K. Takayanagi. 2007. One-by-one evolution of conductance channel in gold [110] nanowires. J. Phys. Soc. Jpn. **76**: 123601 (4pp).

[Kurui *et al.* 2008] Kurui. Y., Y. Oshima, M. Okamoto and K. Takayanagi. 2008. Integer conductance quantization of gold atomic sheets Phys. Rev. B **77**: 161403(R) (4pp).

[Kwon *et al.* 1994] Kwon, I. , R. Biswas, C. Z. Wang, K. M. Ho and C. M. Soukoulis. 1994. Transferable tight-binding models for silicon. Phys. Rev. B **49**: 7242-7250.

[Lin *et al.* 2005] Lin, J.-S., S.-P. Ju, and W.-J. Lee. 2005. Mechanical behavior of gold nanowires with a multishell helical structure. Phys. Rev. B **72**: 085448 (6pp).

[Mares *et al.* 2004] Mares, A. I., A. F. Otte, L. G. Soukiassian, R. H. M. Smit, and J. M. van Ruitenbeek. 2004. Observation of electronic and atomic shell effects in gold nanowires. Phys. Rev. B **70**: 073401 (4pp).

[Mares *et al.* 2005] Mares, A. I. and J. M. van Ruitenbeek. 2005. Observation of shell effects in nanowires for the noble metals Cu, Ag, and Au. Phys. Rev. B **72**: 205402 (7pp).

[Martin 2004] Martin, R. M. 2004. *Electronic Structure: Basic Theory and Practical Methods.* Cambridge University Press, Cambridge.

[Mehl and Papaconstantopoulos 1996] Mehl, M. J. and D. A. Papaconstantopoulos. 1996. Applications of a tight-binding total-energy method for transition and noble metals: Elastic constants, vacancies, and surfaces of monatomic metals. Phys. Rev. B **54**:4519-4530.

[Muller *et al.* 1996] Muller, C. J., J. M. Krans, T. N. Todorov, M. A. Reed. 1996. Quantization effects in the conductance of metallic contacts at room temperature. Phys. Rev. B **53**: 1022-1025.

[Nath and Anderson 1990] Nath, K. and A. B. Anderson. 1990. Atom-superposition and

electron-delocalization tight-binding band theory. Phys. Rev. B **41**: 5652-5660.

[Okamoto and Takayanagi 1999] Okamoto M. and K. Takayanagi. 1999. Structure and conductance of a gold atomic chain. Phys. Rev. B**60**: 7808-7811.

[Ohnishi and Takayanagi 1998] Ohnishi, H., Y. Kondo and K. Takayanagi. 1998. Quantized conductance through individual rows of suspended gold atoms. Nature **395**: 780-785.

[Olesen *et al.* 1994] Olesen, L., E. Lgsgaard, I. Stensgaard and F. Besenbacher. 1994. Quantised conductance in an atom-sized point contact Phys. Rev. Lett. **72**: 2251-2254.

[Ono and Hirose 2005] Ono, T., and K. Hirose. 2005. First-Principles Study of Electron-Conduction Properties of Helical Gold Nanowires. Phys. Rev. Lett. **94**: 206806 (4pp).

[Oshima and Miyano 1998] Oshima, H. and K. Miyano. 1998. Spin-dependent conductance quantization in nickel point contacts. Appl. Phys. Lett. **73**: 2203-2205.

[Oshima *et al.* 2002] Oshima, Y. H. Koizumi,K. Mouri, H. Hirayama, K. Takayanagi, Y. Kondo. 2002. Evidence of a single-wall platinum nanotube. Phys. Rev. B **65**, 121401(R).

[Oshima *et al.* 2003a] Oshima, Y., K. Mouri, H. Hirayama and K. Takayanagi. 2003. Development of a miniature STM holder for study of electronic conductance of metal nanowires in UHV-TEM. Surf. Sci. **531**: 209-216.

[Oshima *et al.* 2003b] Oshima, Y., A. Onga and K. Takayanagi. 2003. Helical Gold Nanotube Synthesized at 150 K. Phys. Rev. Lett. **91**: 205503.

[Oshima *et al.* 2003c] Oshima, Y., Y. Kondo and K. Takayanagi. 2003. High-resolution ultrahigh-vacuum electron microscopy of helical gold nanowires: junction and thinning process. J. Electron Microsc. **52**: 49-55.

[Oshima *et al.* 2006] Oshima, Y., K. Mouri, H. Hirayama and K. Takayanagi. 2006. Quantized Electrical Conductance of Gold Helical Multishell Nanowires. J. Phys. Soc. Jpn. **75**: 053705 (4pp).

[Papaconstantopoulos and Mehl 2003] Papaconstantopoulos, D. A. and M. J. Mehl. 2003. The Slater-Koster tight-binding method: a computationally efficient and accurate approach. J. Phys: Condens. Matter. **15**: R413-R440.

[Pascual 1993] Pascual, J.I., J. Mendez, J. Gómez-Herrero, A. M. Baró and N. García 1993. Quantum contact in gold nanostructures by scanning tunneling microscopy Phys. Rev. Lett. **71**: 1852-1855.

[Payne *et al.* 1992] Payne, M. C., M. P. Teter, D.C. Allan, T. A. Arias and J. D. Joannopoulos. 1992. Iterative minimization techniques for ab initio total-energy calculations: molecular dynamics and conjugate gradients. Rev. Mod. Phys. **64**: 1045-1097.

[Rubio-Bollinger *et al.* 2004] Rubio-Bollinger, G., P. Joyez, and N. Agraït. 2004. Metallic Ad-

hesion in Atomic-Size Junctions. Phys. Rev. Lett. **93**: 116803 (4pp).

[Rubio *et al.* 1996] Rubio, G., N. Agraït and S. Vieira. 1996. Atomic-sized metallic contacts: mechanical properties and electronic transport. Phys. Rev. Lett. **76**: 2302-2305.

[Sánchez-Portal *et al.* 1999] Sánchez-Portal, D., E. Artacho, J. Junquera, P. Ordejón, A. García, and J. M. Soler. 1999. Stiff monoatomic gold wires with aspinning zigzag geometry. Phys. Rev. Lett.**83**: 3884-3887.

[Schiff 1968] Schiff, L. I. 1968. *Quantum Mechanics* 3. Ed. McGraw-Hill, New York

[Senger *et al.* 2004] Senger, R. T., S. Dag and S. Ciraci. 2004. Chiral Single-Wall Gold Nanotubes. Phys. Rev. Lett. **93**: 196807 (4pp).

[Shinaoka *et al.* 2008] Shinaoka, H., T. Hoshi and T. Fujiwara. 2008. Ill-Contact Effects of d-Orbital Channels in Nanometer-Scale Conductor. J. Phys. Soc. Jpn. **77**:114712 (7pp).

[Shiota *et al.* 2008] Shiota, T. A. I. Mares, A. M. C. Valkering, T. H. Oosterkamp, and J. M. van Ruitenbeek. 2008. Mechanical properties of Pt monatomic chains. Phys. Rev. B **77**: 125411 (5pp).

[Smit *et al.* 2003] Smit, R. H. M., C. Untiedt, G. Rubio-Bollinger, R. C. Segers, and J. M. van Ruitenbeek. 2003. Observation of a parity oscillation in the conductance of atomic wires. Phys. Rev. Lett. **91**: 076805 (3pp).

[Sorensen *et al.* 1998] Sorensen, M. R., M. Brandbyge, and K. W. Jacobsen. 1998. Mechanical deformation of atomic-scale metallic contacts: structure and mechanisms. Phys. Rev. B**57**: 3283-3294.

[Takayama *et al.* 2004] Takayama, R., T. Hoshi and T. Fujiwara. 2004. Krylov subspace method for molecular dynamics simulation based on large-scale electronic structure theory. J. Phys. Soc. Jpn. **73**: 1519-1524.

[Takayama *et al.* 2006] Takayama, R., T. Hoshi, T. Sogabe, S-L. Zhang and T. Fujiwara. 2006. Linear algebraic calculation of the Green 's function for large-scale electronic structure theory. Phys. Rev. B**73**:165108 (9pp).

[Todorov *et al.* 1993] Todorov T. N. and A. P. Sutton. 1993. Jumps in electronic conductance due to mechanical instabilities. Phys. Rev. Lett.**70**: 2138-2141.

[Tosatti *et al.* 2001] Tosatti, E., S. Prestipino, S. Kostlmeier, A. Dal Corso and F. D. Di Tolla. 2001. String tension and stability of magic tip-suspended nanowires. Science **291**: 288.

[Urban *et al.* 2004] Urban, D.F., J. Bürki,C.-H. Zhang, C. A. Stafford and Hermann Grabert. 2004. Jahn-Teller distortions and the supershell effect in metal nanowires. Phys. Rev. Lett. **93**:186403 (4pp).

[Valkering *et al.* 2005] Valkering, A. M. C., A. I. Mares, C. Untiedt, K. Babaei Gavan, T. H.

Oosterkamp, and J. M. van Ruitenbeek. 2005. A force sensor for atomic point contacts. Rev. Sci. Instrum. **76**: 103903 (5pp).

[Van Hove *et al.* 1981] Van Hove, M. A., R.J. Koestner, P.C. Stair, J.P. Biberian, L.L. Kesmodel, I. Bartos, G.A. Somorjai. 1981. The surface reconstructions of the (100) crystal faces of iridium, platinum and gold - I. Experimental observations and possible structural models. Surf. Sci. **103**: 189-217

[Xu *et al.* 1992] Xu, C. H. and C. Z. Wang and C. T. Chan and K. M. Ho. 1992. A transferable tight-binding potential for carbon. J. Phys. Condens. Matter **4**: 6047-6054.

[Yang *et al.* 2004] Yang, C.-K. 2004. Theoretical study of the single-walled gold (5,3) nanotube. Appl. Phys. Lett. **85**: 2923-2925.

[Yanson *et al.* 1999] Yanson, A. I., I. K. Yanson and J. M. van Ruitenbeek. 1999. Observation of shell structure in sodium nanowires. Nature **400**: 144-146.

[Yanson *et al.* 2000] Yanson, A.I., I.K. Yanson, J.M. van Ruitenbeek. 2000. Supershell structure in alkali metal nanowires. Phys. Rev. Lett. **84**: 5832-5835.

[Yanson *et al.* 2001] Yanson, A.I., I.K. Yanson, J.M. van Ruitenbeek. 2001. Crossover from electronic to atomic shell structure in alkali metal nanowires Phys. Rev. B **70**: 073401 (4pp).

[Yanson *et al.* 2008] Yanson, I. K., O. I. Shklyarevskii, J. M. van Ruitenbeek, and S. Speller. 2008. Aluminum nanowires: Influence of work hardening on conductance histograms. Phys. Rev. B**77**: 03411 (4pp).